



# Simulation of the future sea level contribution of Greenland with a new glacial system model

Reinhard Calov<sup>1</sup>, Sebastian Beyer<sup>1,2,3</sup>, Ralf Greve<sup>4</sup>, Johanna Beckmann<sup>1</sup>, Matteo Willeit<sup>1</sup>, Thomas Kleiner<sup>2</sup>, Martin Rückamp<sup>2</sup>, Angelika Humbert<sup>2,3</sup>, and Andrey Ganopolski<sup>1</sup>

<sup>1</sup>Potsdam Institute for Climate Impact Research, Earth System Analysis, Potsdam, Germany

<sup>2</sup>Alfred Wegener Institute, Helmholtz Centre for Polar and Marine Research, Bremerhaven, Germany

<sup>3</sup>University of Bremen, Bremen, Germany

<sup>4</sup>Institute of Low Temperature Science, Hokkaido University, Sapporo, Japan

*Correspondence to:* Reinhard Calov (calov@pik-potsdam.de)

**Abstract.** We introduce the coupled model of the Greenland glacial system IGLOO 1.0, including the polythermal ice sheet model SICOPOLIS (version 3.3) with hybrid dynamics, the model of basal hydrology HYDRO and a parameterization of submarine melt for marine-terminated outlet glaciers. Aim of this glacial system model is to gain a better understanding of the processes important for the future contribution of the Greenland ice sheet to sea level rise under future climate change scenarios.

5 The ice sheet is initialized via a relaxation towards observed surface elevation, imposing the palaeo-surface temperature over the last glacial cycle. As a present-day reference, we use the 1961-1990 standard climatology derived from simulations of the regional atmosphere model MAR with ERA reanalysis boundary conditions. For the palaeo-part of the spin-up, we add the temperature anomaly derived from the GRIP ice core to the years 1961-1990 average surface temperature field. For our projections, we apply surface temperature and surface mass balance anomalies derived from RCP 4.5 and RCP 8.5 scenarios

10 created by MAR with boundary conditions from simulations with three CMIP5 models. The hybrid ice sheet model is fully coupled with the model of basal hydrology. With this model and the MAR scenarios, we perform simulations to estimate the contribution of the Greenland ice sheet to future sea level rise until the end of the 21st and 23rd centuries. Further on, the impact of elevation–surface mass balance feedback, introduced via the MAR data, on future sea level rise is inspected. In our projections, we found the Greenland ice sheet to contribute to global sea level rise between 1.9 and 13.0 cm until the year 2100

15 and between 3.5 and 76.4 cm until the year 2300, including our simulated additional sea level rise due to elevation–surface mass balance feedback. Translated into additional sea level rise, the strength of this feedback in the year 2100 varies from 0.4 to 1.7 cm, and in the year 2300 it ranges from 1.7 to 21.8 cm. Additionally, taking Helheim and Store Glaciers as examples, we investigate the role of ocean warming and surface runoff change for the melting of outlet glaciers. It shows that ocean temperature and subglacial discharge are about equally important for the melting of the examined outlet glaciers.

## 20 1 Introduction

Since the last decade of the 20th century, the Greenland ice sheet (GrIS) loses mass with accelerating speed (Helm et al., 2014), shaping one of the most important contributors to sea level rise (Rietbroek et al., 2016). This mass loss is not only driven by



decreasing surface mass balance but also by increasing ice discharge via outlet glaciers (van den Broeke et al., 2016). The partition between these two contributions to GrIS mass loss is about equal (Enderlin et al., 2014). Understanding the processes determining the GrIS ice loss is vital for estimates of its contribution to future sea level rise.

Nowadays, the scientific community recognizes the large Greenland island as a complex system mainly composed of the ice sheet and numerous outlet glaciers (Joughin et al., 2010; Rignot and Mouginot, 2012), in subtle interaction with the surrounding ocean via fjord circulation (Straneo et al., 2012; Murray et al., 2010), and uprising meltwater plumes in interplay with the calving outlet glaciers (O’Leary and Christoffersen, 2013). In our paper, we introduce the model IGLOO (Ice sheet model for Greenland including Ocean and Outlet glaciers, Fig. 1) thought to represent the major processes important for the future mass changes of the GrIS on timescales of some centuries. The idea of this model is to capture the complexity of the system by its involved model components and, at the same time, treating the description of all single components as detailed as necessary (Claussen et al., 2002). We aim to have a tool which is sufficiently fast to enable large ensemble simulations on timescales important for future climate change.

Knowledge of the present-day state of the GrIS has been improving considerably. Not only that there are reliable data from numerous observations (e. g. Velicogna and Wahr, 2005; Bales et al., 2009; Morlighem et al., 2014), but also several modelling studies exist. Present-day GrIS velocities are resolved by ice sheet models in horizontal resolutions as high as 600 m, including flow patterns of outlet glaciers (Aschwanden et al., 2016). Robinson et al. (2012) explicitly demonstrated the multistable-hysteresis behaviour of the GrIS with a threshold of 1.6 °C above present-day global temperature for the decay of the GrIS; although such a decay will last at least about 1000 years. The past climate is an important element for GrIS ice sheet modelling as well, as it can serve as constraint for parameters particularly capturing the present-day GrIS (Robinson et al., 2011; Stone et al., 2013) and as it provides the history of the temperature field inside the present-day GrIS (Goelzer et al., 2013), which is important for the initialization of the GrIS in future warming simulations. However, palaeo-simulations with free surface have the drawback that their resulting present-day elevation can differ considerably from observations (e. g. Calov et al., 2015). Such a simulated elevation is an unfavourable initial condition for projections because, in this case, the future simulation would start with ice which resides at the wrong locations or is absent at position where it should reside due to observations. This leads to an erroneous drift in projected ice volume evolution. Therefore, we opt for a fixed domain approach (Calov and Hutter, 1996) in our palaeo-spin-ups or, more precisely, for a scheme that relaxes the simulated surface elevation towards the observed one (Aschwanden et al., 2013). This approach has the advantage of yielding in a good approximation the present-day temperature-velocity field for initialization and at the same time avoiding spurious response in ice volume during future simulations of some hundred years. Different initialization methods are discussed by Saito et al. (2016).

There are several approaches to project future ice mass change of the GrIS, often with a special focus on a certain component of the Greenland glacial system. Classical surface mass balance approaches assume a passive ice sheet, but resolve the atmosphere with general circulation models of the atmosphere (e. g. Gregory and Huybrechts, 2006) or additionally with a regional model (van Angelen et al., 2012; Fettweis et al., 2013). Several pioneering studies used three-dimensional dynamic ice sheet models in the shallow ice approximation (SIA) for projections of GrIS sea level contribution (e. g. Huybrechts and de Wolde, 1999; Greve, 2000). Later, higher-order (Fürst et al., 2013) or even full-Stokes (Gillet-Chaulet et al., 2012; Seddik et al., 2012)



ice dynamics was included for GrIS future projections. In a higher-order ice sheet model, Fürst et al. (2015) parameterizes ice sliding via ocean-temperature rise due to future climate change to investigate the impact of ocean warming on future projections of GrIS sea level contribution. Studies with an atmosphere-ocean general circulation model coupled to a SIA ice sheet model via surface-energy fluxes were undertaken by Vizcaino et al. (2015). Inspections of GrIS sea level contribution with a special focus on outlet glaciers were accomplished with a 3-D ice sheet model by Peano et al. (2017) or with a 1-D shallow shelf model (Nick et al., 2013).

Here, we opt for the new version of SICOPOLIS v3.3 (Bernales et al., 2017). This version includes hybrid dynamics, which incorporates via the shelfy stream approximation (SSStA; MacAyeal, 1989) longitudinal and lateral stresses, which are important for nearer-margin fast flow areas, along with horizontal plane shear (Hindmarsh, 2004) via the shallow ice approximation (SIA), important for the slow-flow regions in the more central regions of the ice sheet. Hybrid models have been developed before by Pollard and DeConto (2007, 2012); Bueler and Brown (2009); Hubbard et al. (2009); Winkelmann et al. (2011); Fürst et al. (2013); Pattyn (2017). They are a compromise between the shallow ice approximation and the full-Stokes approach. Key of these hybrid models is that SIA and SSStA operate on a common domain, although there are other approaches to treat longitudinal and lateral stresses (Ritz et al., 2001). Compared to the SIA, the hybrid dynamics is more promising in reproducing the velocity field of the GrIS in the catchment area of ice streams, where there is already fast flow (Rignot and Mouginot, 2012).

Models assuming a basal water layer for treatment of subglacial hydrology (Shreve, 1972) were often applied to the Antarctic ice sheet (Le Brocq et al., 2009; Kleiner and Humbert, 2014). Here, we apply such a model to the GrIS, because it captures the major pathways of basal water toward the outlet glaciers (Livingstone et al., 2013), i. e. the model resolves in a good approximation the partition of basal water for the main GrIS outlet glaciers. This is important for reproducing the subglacial discharge of outlet glaciers, which is input for our model of their meltwater plumes. Further on, our model for basal hydrology simulates a thickening of the basal water layer toward the major GrIS outlet glaciers, regions over which the ice velocity becomes higher (Rignot and Mouginot, 2012). Therefore, we couple the ice velocities to the basal water layer, while the basal melt rate of the ice sheet model provides the input to the model of basal hydrology. We expect this approach of being capable for large-scale ice sheet modelling on decadal timescales.

Simulating submarine melt rates at tidewater glaciers has been accomplished with different models that all share the core of the buoyant-plume theory (Sciascia et al., 2013; Xu et al., 2013; Slater et al., 2015; Carroll et al., 2015; Cowton et al., 2015; Slater et al., 2017). Recent studies (Jackson et al., 2017; Beckmann et al., 2017) show that the line plume model by Jenkins (2011) is an adequate tool to determine submarine melt rates for tidewater glaciers. In our paper, we apply a recently developed line plume model (Beckmann et al., 2017) after the equations of Jenkins (2011) to two outlet glaciers, Store and Helheim Glaciers, of the Greenland ice sheet. We have chosen Helheim and Store Glaciers for investigating the impact of future warming on glacier melt and for testing our methods because they are well examined glaciers: Numerous studies on these glaciers and their connecting fjord systems to the open ocean exist (Straneo et al., 2011; Sutherland and Straneo, 2012; Rignot et al., 2015; Jackson et al., 2014; Chauché et al., 2014). Some provide data on temperature- and salinity profiles inside the fjord from conductivity-temperature-depth (CTD) measurements or moorings.



We start with a description of the elements of the glacial system model IGLOO 1.0, including the future and past forcings utilized in our paper (Section 2). In Section 3, we describe our initialization method, while Section 4 compares the simulated present-day surface elevation and velocity with observations. Further on, modelled basal properties are compared with findings of other works. In Section 5, we present projections of GrIS sea level contribution, of GrIS total basal and surface runoff and of the submarine melt rates for two GrIS outlet glaciers (Store and Helheim Glaciers). The paper closes with a discussion (Section 6) and the conclusions (Section 7).

## 2 Ice sheet model for Greenland including ocean and outlet glaciers (IGLOO), version 1.0

### 2.1 Ice sheet model SICOPOLIS version 3.3

SICOPOLIS (SIMulation COde for POLythermal Ice Sheets; [www.sicopolis.net](http://www.sicopolis.net)) is a dynamic/thermodynamic ice sheet model that was originally created by Greve (1995, 1997) in a version for the GrIS. Since then, SICOPOLIS has been developed continuously and applied to problems of past, present and future glaciation of Greenland (e.g., Robinson et al., 2011), Antarctica (e.g., Kusahara et al., 2015), the Eurasian ice sheet including subglacial water (Gudlaugsson et al., 2017), the entire Northern hemisphere (Ganopolski and Calov, 2011), the polar ice caps of the planet Mars and others (see [www.sicopolis.net/publ](http://www.sicopolis.net/publ) for a comprehensive publication list). The description given here follows Greve et al. (2017) very closely.

The model simulates the large-scale dynamics and thermodynamics (ice extent, thickness, velocity, temperature, water content and age) of ice sheets three-dimensionally and as a function of time. It is based on the shallow ice approximation for grounded ice (Hutter, 1983; Morland, 1984) and the shallow shelf approximation for floating ice (Morland, 1987; MacAyeal, 1989). Recently, hybrid shallow-ice/shelfy-stream dynamics has been added as an option for ice streams (Bernales et al., 2017). The rheology is that of an incompressible, heat-conducting, power-law fluid (Glen's flow law; e.g., Greve and Blatter, 2009).

A particular feature of SICOPOLIS is its very detailed treatment of ice thermodynamics. A variety of different thermodynamics solvers are available, namely the polythermal two-layer method, two versions of the one-layer enthalpy method, the cold-ice method and the isothermal method (Greve and Blatter, 2016). The polythermal and enthalpy methods account in a physically adequate way for the possible co-existence of cold ice (with a temperature below the pressure-melting point) and temperate ice (with a temperature at the pressure-melting point) in the ice body, a condition that is referred to as "polythermal". It is hereby assumed that cold ice makes up the largest part of the ice volume, while temperate ice exists as thin layers overlying a temperate base. In the temperate ice layers, the water content is computed, and its reducing effect on the ice viscosity is taken into account (Lliboutry and Duval, 1985).

SICOPOLIS is coded in Fortran and uses finite difference discretization techniques on a staggered Arakawa C grid, the velocity components being taken between grid points (Arakawa and Lamb, 1977). For solving the thickness evolution equation, we added a further option to the SICOPOLIS code (Appendix A). The simulations of the GrIS discussed here are carried out in a stereographic plane (WGS 84 reference ellipsoid, standard parallel 71°N, central meridian 39°W), spanned by the Cartesian coordinates  $x$  and  $y$ . The coordinate  $z$  points upward.



## 2.2 Subglacial hydrology model HYDRO

Subglacial water flux and storage are governed by the hydraulic potential  $\Phi$ , which depends on the elevation potential and the water pressure  $p_w$  (Shreve, 1972):

$$\Phi = \rho_w g b + p_w, \quad (1)$$

5 with the ice base  $b$ , acceleration due to gravity  $g$  and density of water  $\rho_w = 1000 \text{ kg m}^{-3}$ . The water pressure depends on the ice overburden pressure and the effective pressure  $N$  (normal stress at the bed minus water pressure):

$$p_w = \rho_i g H - N, \quad (2)$$

wherein  $\rho_i = 910 \text{ kg m}^{-3}$  is the density of ice.

Following previous authors such as Le Brocq et al. (2009) and Livingstone et al. (2013), we assume the water moving in  
10 a thin (a few mm) and distributed water film. Under this premise, the water pressure and the ice overburden pressure are in equilibrium and therefore the effective pressure is zero. This enables us to reformulate Eq. (1) as

$$\Phi = \rho_w g b + \rho_i g H, \quad (3)$$

and then computing the water flux with a simple flux routing scheme as described by Le Brocq et al. (2006). This approach is only valid at large (km) scales and is not able to include local processes such as channels.

15 The flux routing method requires that every cell has a defined flow direction and that, by successively following these directions, the boundary of the study area is reached. Therefore, local sinks and flat areas must be removed prior to applying the routing scheme. We accomplish this by using a Priority-Flood algorithm as described in Barnes et al. (2014), which fills depressions in a single pass and then add a small gradient to the resulting flats. Adding a gradient towards the outlet of the depression ensures that the hydraulic potential is altered in the smallest possible way. This procedure is a very efficient way to  
20 guarantee that all water is drained into the ocean.

The hydraulic potential is computed following Eq. 1, and we use the basal melt rates from SICOPOLIS as the water input for the routing scheme (see Section 2.4.1). The timescales of the water flow are much smaller than for the ice flow, thus, the steady-state water flux  $\psi_w$  can be obtained by integrating the basal melt rate along the hydraulic potential.

From the resulting water flux  $\psi_w$ , we can compute the water layer thickness  $W$  (Weertman, 1972, 1966):

$$25 \quad W = \left( \frac{12 \mu_w \psi_w}{\text{grad } \Phi} \right)^{1/3}. \quad (4)$$

At locations where sinks in the hydraulic potential have been filled, we set  $W$  to a very high value (10 m) to account for the presence of a subglacial lake.

## 2.3 Meltwater plume model

A further element of IGLOO is the line plume model by Beckmann et al. (2017) (after Jenkins (2011)). It simulates the width-  
30 averaged submarine melt rate of a glacier and accounts for a uniformly distributed subglacial discharge along the grounding



line. The plume model describes buoyancy-driven rise of subglacial meltwater until it reaches either neutral buoyancy or the water surface. Two counteracting processes control the maintenance or reduction of the plume buoyancy: Submarine melting at the ice-ocean interface preserves the plume buoyancy, while simultaneously turbulent entrainment and mixing with the surrounding salty fjord water reduces it. The line plume equations are derived under the assumption that the plume is in equilibrium and are thus time-independent. The melt rate is determined by the plume velocity and temperature, which adapts to the boundary conditions along the glacier front or under the floating tongue. As input parameters, it requires the grounding line depth  $Z$  ( $Z < 0$ ), the shape of the glacier front, the subglacial discharge  $Q$  that leaves the glaciers grounding line over the whole glacier width, and a temperature-salinity depth (TSD) profile close to the glacier. The determination of the input parameters of the plume model is described in section 2.4.2.

## 10 2.4 Coupling of model components

### 2.4.1 Coupling of SICOPOLIS with HYDRO

We use a slightly modified version of the Weertman-type sliding law proposed by Kleiner and Humbert (2014) to couple the basal hydrology model to the ice dynamics:

$$v_b = -f_b C_b |\tau_b|^{p-1} \tau_n^{-q} \tau_b, \quad (5)$$

15 with the sliding velocity  $v_b$ , basal sliding parameter  $C_b$ , basal shear stress  $\tau_b$ , basal normal pressure  $\tau_n$  (assumed as the ice overburden pressure) and the stress and pressure exponents  $p = 3$  and  $q = 2$ . We introduce the dimensionless factor

$$f_b = f_T ((1 - c_w) + c_w f_w), \quad c_w \in [0, 0.9], \quad (6)$$

with

$$f_T = \exp(\nu(T - T_{\text{pmp}})) \quad \text{and} \quad f_w = \left(1 - \exp\left(-\frac{W}{W_0}\right)\right), \quad (7)$$

20 where  $f_T$  and  $f_w$  incorporate sub-melt sliding and basal hydrology respectively. Sub-melt sliding allows sliding below the pressure melting point  $T_{\text{pmp}}$  according to the decay parameter  $\nu$  (Hindmarsh and Le Meur, 2001), whereas the basal hydrology term depends on the water layer thickness  $W$  divided by a typical scale of the layer thickness  $W_0$ .

The parameter  $c_w$  in Eq. 6 is a weighting factor between “background sliding” – determined by  $C_b$  – and enhanced sliding due to the basal water layer. Using  $c_w = 0$  yields the standard model without any effect of basal hydrology, while  $c_w = 0.9$  leads to the same expression as Kleiner and Humbert (2014). In our simulation with basal hydrology, we apply their parameter value, i. e. we set  $c_w = 0.9$ , while we specify the typical scale of the layer thickness by  $W_0 = 0.005$  m. Further, our decay parameter is  $\nu = 1^\circ\text{C}$ .

The coupling is bi-directional. Basal melt (including the water drainage from the temperate basal layer of the ice sheet) computed by SICOPOLIS is used to calculate the thickness of the basal water layer in HYDRO, which in turn affects the basal sliding (Eq. 7). Components and data exchange of the complete coupled model IGLOO are illustrated in Fig. 1.



#### 2.4.2 Off-line coupling of SICOPOLIS and HYDRO with the plume model

We establish a procedure of determining submarine melt rates with our line plume model (Section 2.3) for all Greenland outlet glaciers. This procedure applies only off-line yet, i. e., the input and output of the model components are exchanged manually via data files.

- 5 For the required subglacial discharge, we use HYDRO to route the basal melt of SICOPOLIS to the grounding line of the glaciers. The grounding line position of each glacier is determined by the ice-land mask of SICOPOLIS of the year 1900 closest to the coordinates by Rignot and Mouginot (2012).

Furthermore, we assume that the surface melt/runoff penetrates directly down to the bedrock and route it from there as basal water to the grounding lines. To clarify, as this coupling is off-line, the sliding of ice (Section 2.4.1) is affected solely by basal melt, while the surface melt and basal melt can impact the meltwater plume. Thus, with a method based on distance criteria, the basal water is routed to the determined grounding line position of each glacier and enters the corresponding fjords as subglacial discharge. We route on a monthly timescale to resolve seasonality. Although we simulate future scenarios, the grounding line position is considered to be fixed for this procedure. Of course, for glaciers close to another that share the same catchment area, a moving grounding line position might have severe effects. We will account for these dynamic glacier processes in the next version of IGLOO. Despite the assumption of a fixed grounding line, our method is already able to determine the subglacial discharge for each glacier.

#### 2.5 Evaluating the data from the regional atmosphere model MAR

The ice sheet model needs the mean annual surface temperature and surface mass balance (SMB) as climate forcings at the surface. In addition, the plume model requires monthly runoff. We construct our future climate forcing from simulations by the MAR regional climate model (Fettweis et al., 2013). Historical MAR simulations using different climate reanalysis products to define the boundary conditions for the regional simulations are available. The boundary conditions for MAR future projections up to 2100 are provided by the output of several CMIP5 general circulation models for different RCP scenarios. Since the MAR simulations are performed for fixed surface elevation of the GrIS and we expect substantial changes in the ice elevation under future warming scenarios, we correct the regional model output for the change in surface elevation by applying the gradient method of Helsen et al. (2012). In their method, they derived a representative local elevation gradient of the SMB in each grid point from a regression of simulated SMB and surface elevation within a given radius. Helsen et al. (2012) did this separately for accumulation and ablation regimes. Here, we extend their method by applying it also to surface temperature and runoff. The search radius is set to 100 km, but is extended until it includes at least 100 grid points, if necessary. For the surface mass balance, we apply the gradient method only to the ablation regime, because the regression is in many cases not well defined for the accumulation regime (Helsen et al., 2012). Therefore, we set the SMB elevation gradient for the accumulation regime to zero.



## 2.6 Past climate forcing and implied flux of the GrIS

The past climate forcing serves two purposes. First, it is used to determine an initial temperature-velocity field for future warming scenarios, and second, to yield the implied flux for the present day, which is used in our future simulations as the climatological present-day surface mass balance.

- 5 The surface temperature for the past simulation is computed from the sum of the climatological field of the present-day surface temperature simulated by MAR, the temperature anomaly from the GRIP ice core and our temperature elevation correction obtained from the present-day MAR simulations:

$$T_s(x, y, t) = T_{s, \text{MAR(rea)}}^{\text{Clim 1961-1990}}(x, y) + \Delta T_{\text{GRIP}}(t) + \left( \frac{\partial T_s}{\partial z} \right)_{\text{MAR(rea)}}^{\text{Clim 1961-1990}}(x, y) \Delta z(x, y, t). \quad (8)$$

10 The elevation correction in the last term of Eq. 8 is the surface temperature elevation gradient from the MAR reanalysis data times a surface elevation difference, which reads

$$\Delta z(x, y, t) = z(x, y, t) - z_0(x, y), \quad (9)$$

with the surface elevation  $z$ , simulated with the ice sheet model SICOPOLIS, and the observed surface elevation  $z_0$ . For the observed surface elevation, we use the one by Bamber et al. (2013), which is the same as that utilized by Fettweis et al. (2013).

15 Here, the surface mass balance  $M$  is defined by relaxing the ice sheet's surface elevation towards the observed surface elevation as

$$M(x, y, t) = \frac{z_0(x, y) - z(x, y, t)}{\tau_{\text{relax}}}, \quad (10)$$

20 where  $\tau_{\text{relax}}$  is a relaxation constant. With this relaxation method, we follow Aschwanden et al. (2013, 2016). Outside the ice sheet, we assign the high negative value of  $M = -1000$  m ice/yr, which prevents the ice to flow outside its domain. With these forcings, we run the model over one glacial cycle. When the model reaches its present-day state ( $t = 0$ ), we yield the implied flux  $M_{\text{impl}}$  which is used in future simulations as

$$M_{\text{impl}}(x, y) := M(x, y, 0). \quad (11)$$

Through Eq. 10, the simulated surface elevation tends to approach the observed one, with a strength determined by  $1/\tau_{\text{relax}}$ . If  $\tau_{\text{relax}}$  equalled the scheme's time step for its ice sheet topography, the simulated surface elevation would fully match the observed one. This would correspond to a fixed domain, or more precisely, to a fixed surface simulation.

25 We made here the following simplifications: (1) We ignored changes in elevation and spatial extent of the GrIS during the past glacial cycle, (2) we assumed that the GRIP temperature record can be applied to the entire GrIS and (3) we assumed that the derived present-day elevation correction is valid for the entire glacial climate state.

30 Outputs of this procedure are the present-day implied flux and a full nearly present-day topography set (surface and bedrock elevation) belonging to this implied flux. Later on, the present-day implied flux field is added to the anomaly forcing of future climate simulations (see Eq. (13)), as this implied flux field is assumed to be the present-day SMB including the errors of the model.



## 2.7 Future climate forcing of the GrIS

The surface temperature forcing is computed from the climatological temperature of MAR simulations for 1961–1990 forced by the ERA reanalysis boundary conditions, the anomalies from MAR simulations forced by CMIP5 model output and a temperature elevation correction as:

$$5 \quad T_s(x, y, t) = T_s^{\text{Clim } 1961-1990}_{\text{MAR(rea)}}(x, y) + (T_s^{\text{MAR(CMIP5)}}(x, y, t) - T_s^{\text{Clim } 1961-1990}_{\text{MAR(CMIP5)}}(x, y)) \\ + \left( \frac{\partial T_s}{\partial z} \right)_{\text{MAR(CMIP5)}}(x, y, t) \Delta z(x, y, t). \quad (12)$$

Here, the temperature elevation correction is determined via the product of the surface temperature elevation gradient of the MAR model with boundary condition from the CMIP5 models and the elevation anomalies simulated with the ice sheet model SICOPOLIS. As for the palaeoclimate,  $\Delta z(x, y, t)$  are the simulated surface elevation anomalies (Eq. 9).

- 10 The SMB for future projections is computed as the sum of the implied flux, simulated SMB anomalies relative to the reference period 1961–1990 and an elevation SMB correction as follows:

$$M(x, y, t) = M_{\text{impl}}(x, y) + (M_{\text{MAR(CMIP5)}}(x, y, t) - M_{\text{MAR(CMIP5)}}^{\text{Clim } 1961-1990}(x, y)) \\ + \left( \frac{\partial M}{\partial z} \right)_{\text{MAR(CMIP5)}}(x, y, t) \Delta z(x, y, t). \quad (13)$$

- 15 Similar to temperature, the elevation SMB correction is calculated from the SMB elevation gradient of the MAR model with boundary condition from the CMIP5 models, multiplied by the simulated surface elevation anomalies.

Surface runoff is computed for each month from the climatological runoff of MAR simulations for 1961–1990 forced by the ERA reanalysis boundary conditions, the anomalies from MAR simulations forced by CMIP5 models output and a runoff elevation correction, which again is computed similarly to the temperature elevation correction:

$$20 \quad R(x, y, t) = R_{\text{MAR(rea)}}^{\text{Clim } 1961-1990}(x, y) + (R_{\text{MAR(CMIP5)}}(x, y, t) - R_{\text{MAR(CMIP5)}}^{\text{Clim } 1961-1990}(x, y)) \\ + \left( \frac{\partial R}{\partial z} \right)_{\text{MAR(CMIP5)}}(x, y, t) \Delta z(x, y, t). \quad (14)$$

Negative runoff values, which can result from this approach, are set to zero.

- Figure 2 shows time series derived from the MAR data. During the 20th century, all curves show rather minor changes in average, besides a visible climate variability. This is in line with general knowledge (e.g. Box et al., 2009; Box and Colgan, 2013). The climate sensitivity is strongest for CanESM2, weakest for NorESM1, and MIROC5 lies in between. Of course, 25 these 21st century warming trends correspond to IPCC AR5 (Collins et al., 2013) because the MAR forcing is from the CMIP5 models. The annual average temperature change over Greenland is stronger than the global one.

Since for NorESM1 and CanESM2, MAR data are missing for 1900–1949, and we do not have access to any MAR data beyond 2100 (even though we need forcings until 2300), we filled the gaps by an extrapolation method that is explained in more detail in Appendix B.



## 2.8 Future climate forcing of the plume model

As future forcing of the plume model, we employ the subglacial discharge from HYDRO and SICOPOLIS (Section 2.4.2) under the RCP 8.5 scenario (Section 2.7) from MAR with MIROC5 only. Additionally, a scenario of the temperature and salinity profiles is needed to project future submarine melting. Even for the present day, measurements inside fjords are rare and do not cover all of Greenland's fjords. We use CTD profiles close to the glaciers obtained for the year 2016 for Store Glacier (data from NASA's OMG mission(<https://omg.jpl.nasa.gov/portal/>)) and the year 2012 for Helheim Glacier (Carroll et al., 2016). For the ocean warming scenario, we assume a linear temperature trend of 0.03 °C per year over the years 2000–2100 for the entire profiles.

The 3 °C ocean warming in 100 years lies in the upper range found by Yin et al. (2011) for SE and W Greenland. The determined temperature and salinity profiles, in combination with the HYDRO output, serve as the input parameters for the line plume model to determine present and future submarine melting for the Greenland outlet glaciers.

## 3 Model initialization via palaeo-runs

For the initialization of the ice sheet model, we use the forcings for the surface temperature and the surface mass balance as described in Section 2.6. Here, isostatic depression and rebound of the lithosphere due to changing ice load is modelled assuming a local lithosphere with relaxing asthenosphere with an isostatic time lag (LLRA approach, Le Meur and Huybrechts, 1996). For the geothermal heat, we use the spatial dependent data by Purucker (2012). In order to cover one full glacial cycle, we run the model over 135 kyrs. Initial conditions of these runs are the present-day ice thickness and elevation by Bamber et al. (2013). The original data with 1 km × 1 km horizontal resolution are downsampled to 5 km × 5 km and 10 km × 10 km grid spacings. To perform a simulation in 5 km × 5 km horizontal resolution over the entire glacial cycle with the hybrid model is illusive, as it takes 1 day for 100 model years on one HLR2015 Lenovo NeXtScale nx360M5 processor. Therefore, we opt to perform the first 130 kyrs of the glacial cycle in 10 km × 10 km horizontal resolution with the classical shallow ice approximation (SIA) employing the diffusivity method with an over-implicit ice-thickness solver. The last 5 kyr of the palaeo-run are performed in 5 km × 5 km horizontal resolution. As we use different model hierarchies and settings, we devote some more explanation to these last 5 kyr.

During the last 5 kyrs of the run, we have three switches: one for refining the horizontal resolution, one for switching from SIA mode to hybrid mode, and a further one for switching from relaxing ice surface to free ice surface. The first switch at 5 kyr BP refines the horizontal resolution of the model from 10 km × 10 km to 5 km × 5 km. The second switch at 500 years BP changes from SIA to hybrid mode and additionally applies the mass conservation scheme for the evolution equation of ice thickness (Eq. A1). The third switch, which releases the relaxing ice surface to free development, is imposed at 100 years BP (year 1900). We introduced this switch 100 years earlier than the start of our future sea level scenarios (Section 5.1) in order to avoid spurious trends in ice volume change in our scenarios, which can happen when the ice sheet is released to free surface evolution suddenly.



The choice of the relaxation constant rests on numerous simulations in  $10 \text{ km} \times 10 \text{ km}$  horizontal resolution in SIA mode, running the model over one glacial cycle until the present day. Figure 3 shows the root mean square error (RMSE) in surface elevation and the total difference in SMB (the total implied flux over the GrIS minus the total SMB simulated by MAR). With increasing relaxation constant, the RMSE in surface elevation increases moderately, while the total difference in SMB decreases strongly, i. e., there is a tradeoff between the RMSE in elevation and the total difference in SMB.

Figure 4 shows the spatial differences between the observed and modelled surface elevation and SMB for different relaxation constants. Again, the tradeoff for representing both surface elevation and SMB is visible. While the simulated elevation is very close to the observation for small relaxation constants, the SMB deviation is very high, even in the interior of the ice sheet, where the deviations reach the amount of magnitude of the accumulation rate. Therefore, too small relaxation constants should be excluded. For larger relaxation constants, both difference fields become smoother, but rather high deviations in surface elevation appear over vast areas of the GrIS. Therefore, too high relaxation constants should be excluded too.

#### 4 Present-day Greenland ice sheet

Here, we present our optimal simulation of the GrIS using the SICOPOLIS model version 3.3 with hybrid dynamics and the model for basal hydrology (HYDRO). Both models are fully coupled (see Section 2.4.1), and the horizontal resolution is always  $5 \text{ km} \times 5 \text{ km}$  from now on. In the hybrid mode, a threshold of  $r_{\text{thr}} = 0$  applies to the slip ratio (Eq. 8 in Bernales et al. (2017)), i. e., the SStA equations are solved over the entire ice sheet, and the ice velocities are the weighted sum from the SIA and SStA velocities with the slip ratio as weight. The boundary conditions and initialization method to yield the present-day GrIS are described in Sections 2.6 and 3, respectively. As relaxation constant for the surface elevation we use  $\tau_{\text{relax}} = 100$  years. Optimal values for the sliding parameters are found by minimizing the error of simulated horizontal surface velocities for values  $> 50 \text{ m/yr}$ , using observations by Rignot and Mouginot (2012). For such velocities, we expect basal sliding and hybrid ice dynamics to be relevant. We found  $C_b = 25 \text{ m}/(\text{Pa yr})$  to be optimal for the hybrid model with basal hydrology.

By design of the initialization, the simulated surface elevation compares overall well with the observed one, see Fig. 5a,b. However, as our surface relaxation method leaves the ice sheet's surface a certain degree of freedom (see also Fig. 4), the simulated ice surface over Summit and South Dome as well as on the ridge in between them is slightly lower. The simulated surface velocity along the ridges is somewhat smaller compared to the observed one. Such (small) mismatches also appear with other higher-order models, even in higher resolution (Aschwanden et al., 2016). Recall that we adjusted the sliding parameter  $C_b$  to match higher velocities higher than  $50 \text{ m/yr}$  with observations. The model resolves the major flow patterns of the GrIS, including the flow over the catchment area of the outlet glaciers and the fast flow of the major outlet glaciers and ice streams. Only the smaller-scale outlet glaciers, e. g. in north-west Greenland, are not fully resolved. Further, we cannot model outlet glaciers with floating tongues, such as Petermann, Nioghalvfjærdsbræ and Zachariæ Isstrøm. The Northeast Greenland Ice Stream (NEGIS) is the only larger scale feature which we cannot reproduce properly. This feature cannot be simulated without additional assumptions (see the Discussion section).



Figure 6 zooms in Jakobshavn Isbræ and the two major outlet glaciers Helheim and Kangerdlugssuaq. Here, the ability of the model to resolve the catchment areas of these outlet glaciers in a 50 to 500 m/yr range can be seen in more detail. However, the high-velocity patterns near the glacier termini do not fully match the simulations. In particular, the tributaries of Helheim and Kangerdlugssuaq glaciers and the tip of Jakobshavn Isbræ appear rather smooth compared to the observation.

5 Fast flow mainly appears over regions with a temperate ice bed. The simulated basal temperature in Fig. 7a shows a pattern which agrees basically with the reconstruction by MacGregor et al. (2016). Regions where there is basal melt, mainly caused by basal friction, exhibit a 1 to 5 mm thick water layer (Fig. 7b). There is a pronounced thickening of the water layer with our Shreve-flow modelling toward major ice streams and outlet glaciers, which is most visible for NEGIS, Jakobshavn Isbræ and Helheim Glacier. Moreover, smaller outlet glaciers like Store Glacier and Daugaard-Jensen Glacier receive intensified basal  
10 water supply too.

## 5 Greenland glacial system projections

### 5.1 Projections of the GrIS's sea level contribution

For our projections of the contribution of the GrIS to global sea level rise, the GrIS is forced by SMB anomalies and surface temperatures derived from the MAR regional climate model (Section 2.7), making use of the initial ice sheet configurations  
15 explained in Section 3. As for the last 500 years of initialization, the fully coupled hybrid model including basal hydrology is utilized. Outside of the present-day GrIS area, similarly to the initialization, the prohibiting negative SMB is applied. In Fig. 8, we show the GrIS sea level contribution referenced to the year 2000. The control simulation forced solely with the implied flux illustrates the characteristics of our initialization method. Indeed, with this forcing, there is almost no change in ice volume  
20 visible. Only after 300 years, a tiny ice volume change can be detected in Fig. 8b, due to the comparably small scale in the  $y$ -axis therein. This model drift amounts about 2 mm sea level contribution per 100 years. In spite of such a small change, we correct our simulated sea level contribution of the GrIS in the simulation with MAR forcing for the implied-flux-only simulations.

Our projections of the GrIS sea level contribution for the year 2100 are close to simulations with a fixed present-day GrIS applying the cumulative SMB method (Church et al., 2013). This is in line with simulations with an active ice sheet model by  
25 Goelzer et al. (2013), who found that SMB is the major factor determining the GrIS sea level contribution over the 21st century. Our simulated GrIS sea level contribution for 2100 ranges from 1.9 cm (RCP 4.5, NorESM1) to 13.0 cm (RCP 8.5, CanESM2), see Table 2. Still, the ice dynamics (deformation and sliding velocities) plays a role in our simulations, indirectly via the SMB change. This can be seen when comparing the simulations with and without elevation SMB correction ( $\partial M / \partial z$ )  $\Delta z$ , Eq. 13. Ignoring the elevation SMB correction diminishes simulated 21st-century GrIS sea level contribution between 0.4 and 1.7 cm.  
30 Of course, this effect is strongest for the extreme RCP 8.5 scenario together with CanESM2, the CMIP5 model exhibiting the most climate sensitivity.

Certainly much stronger than for the 21st century, the sea level contribution of the GrIS for the year 2300 ranges from 3.5 cm to 76.4 cm. The importance of the elevation SMB feedback clearly increases with the elapsed time of the projections, as



the respective curves with  $\partial M/\partial z$  on/off diverge more and more from each other. For RCP 8.5 with CanESM2, the relative increase of additional loss in ice volume due to elevation SMB correction nearly triples from 2100 to 2300, from 15% to 40%. Detailed numbers for the sea level contributions of the GrIS for the years 2100 and 2300 are listed in Table 2.

Overall, our simulations show a strong dependence of the GrIS sea level contribution both on the RCP scenarios and on the model used to force MAR. Besides, the impact of the description of ice dynamics on the GrIS sea level rise contribution – i. e., whether SIA or hybrid is used – is minor, although the velocities over the catchment areas of the ice streams are better represented in the hybrid model compared to the SIA model (not shown).

## 5.2 Projections of the GrIS's total basal and surface runoff

For these projections, we use the basal melt from the two simulations by SICOPOLIS (Section 5.1) forced by the MAR data for which MAR used the MIROC5 GCM under the RCP 8.5 scenario. Surface and basal melt are routed over the ice base and distributed to the GrIS outlet glaciers. The details are explained in Section 2.4.2. Figure 9 depicts the total subglacial discharge split into surface runoff and basal melt. The total basal melt amounts to about 15 Gt per year, while the surface runoff increases up to 1700 Gt per year. Note that, after the year 2100, the surface runoff is decreasing due to the shrinking ice sheet area. Simultaneously, the effect of the elevation SMB feedback becomes more important after the year 2100, leading to much higher surface runoff than without the feedback (Eq. 14).

## 5.3 Projections of submarine melt rate for the GrIS outlet glaciers Helheim and Store

Here, we inspect the impact of global warming under the RCP 8.5 scenario for two outlet glaciers: Helheim Glacier and Store Glacier. In detail, we analyse the impact of both subglacial discharge and ocean warming – as single and combined effects – on the submarine melt rate of these outlet glaciers. While the subglacial discharge comes from simulations with SICOPOLIS and HYDRO under the RCP 8.5 scenario, the ocean warming originates from a scenario similar to RCP 8.5 (Section 2.8). For analysing the impact of the elevation SMB feedback on submarine melt, the plume model is forced by subglacial discharge computed with and without the surface elevation correction of surface runoff (Eq. 14). We calculate all submarine melt rates under the assumptions of both glaciers being tidewater glaciers (no floating tongues) and of their grounding-line depths and widths remaining constant in time. These depths and widths are acquired from present-day observations and amount to 500 m depth and 5 km width for Store Glacier (Chauché et al., 2014) and 650 m depth (Carroll et al., 2016) and 6 km width (Straneo et al., 2016) for Helheim Glacier. We chose the entrainment parameter to be  $E_0 = 0.036$  as recommended by Beckmann et al. (2017).

Figures 10 and 11 illustrate the monthly subglacial discharge and the temperature profiles for the years 2000 and 2100 and the resulting submarine melt rates for the RCP 8.5 scenario. For both glaciers, the increasing subglacial discharge and the increasing ocean temperature have an about equal effect on the rising submarine melt, with the ocean temperature becoming more important towards the end of the year 2100. However, the combined effect of increased subglacial discharge and temperature exceeds the single effects alone. As a result, submarine melt exhibits a 2.5-fold increase for Helheim Glacier and a 4-fold increase for Store Glacier in the year 2100 (Figs. 10c and 11c). Although for the year 2000 the amount of basal melt ( $38 \text{ m}^3/\text{s}$



for Helheim, 5 m<sup>3</sup>/s for Store) is small compared summer subglacial discharge (818 m<sup>3</sup>/s for Helheim, 439 m<sup>3</sup>/s for Store), it has a significant effect on the annual submarine melt rate. Due to the basal melt in the winter months (including early spring and late autumn), the submarine melt rate enlarges in those months substantially as illustrated by Fig. 12 for Helheim Glacier. The slight increase in subglacial discharge for all months (Fig. 12a) shows clearly the biggest increase in submarine melt rate  
5 for the winter months (Fig. 12b) due to the cubic root dependence of submarine melt rate on subglacial discharge (Jenkins, 2011). On the annual average, this effect leads, for the year 2000, to an increase of submarine melt for Helheim Glacier by 40% and for Store Glacier by 20% compared to the case when basal melt was not accounted for (Figs. 10c and 11c). The missing effect of surface elevation correction does not show big impacts on submarine melt rate when turned off (Figs. 10c and 11c). However, as Fig. 9 suggests, this effect will become more important after the year 2100.

10 In these experiments, the future submarine melt rate was calculated assuming a constant glacier terminus position and geometry. These calculation have to be seen as a first approximation because we neglect several factors that may influence the submarine melt rate. For instance, if the glacier retreats, the resulting grounding line depth may change depending on the underlying bedrock. Another factor that might change the melt rate estimation considerably is the distribution of subglacial discharge within the year. Here, we assumed no time lag in between runoff and its emergence as subglacial discharge. Due  
15 to the cubic root dependence of submarine melting on subglacial discharge, we already see the possible strong effect of basal runoff from the ice sheet on the distribution of the submarine melt rate of an outlet glacier over the year (see Fig. 12). Thus, an inefficient drainage system that is delayed by, e. g., storage of water in subglacial lakes (Nienow et al., 2017) might affect the seasonal distribution of subglacial discharge and thus the annual submarine melt rate substantially.

## 6 Discussion

20 In Section 3, we investigated the role of the relaxation constant for initialization. For very small relaxation constants, i. e., an essentially fixed ice surface, the difference between implied and observed SMB at present day becomes very large (more than 2000 Gt/yr, compared to an insignificant amount for  $\tau_{\text{relax}} = 100$  years). Note that the present-day magnitude of observed total SMB is only about 500 Gt/yr (e. g. Ettema et al., 2009). This means that computation with fully fixed surface should be treated with care, as the total artificial mass needed to keep the ice sheet close to observation is very high. A further factor is a smooth  
25 surface elevation, the importance of which was already observed earlier by Calov and Hutter (1996).

In our simulations, we cannot reproduce the NEGIS ice stream correctly. Certainly, one reason is that we do not optimize the surface velocity by a spatially dependent basal sliding coefficient. With spatially dependent basal sliding coefficients, other studies such as Price et al. (2011) and more recently Peano et al. (2017) simulated the NEGIS in better agreement with observations. Nowadays, there are process-oriented approaches to capture effects important for basal sliding. For example,  
30 stronger basal melting at the onset of the NEGIS caused by increased geothermal heat due to a palaeo-hotspot (Rogozhina et al., 2016) could be one factor speeding up the simulated NEGIS velocity. A further factor can be a deepening of the basal topography in this region (Vallelonga et al., 2014).



For our 300-year sea level projections, which reach beyond the 21st century, we prolong the forcing data of the MAR model until the year 2300. Because we merely held the forcing constant between 2101 and 2300, the real RCP 8.5 forcing could be larger, i.e., we expect our simulations with the RCP 8.5 scenario to be a lower estimate of sea level contribution of the GrIS, i.e., the estimate is a rather conservative one. Most certainly, even all our projections including RCP 4.5 are a conservative  
5 estimate, because a full coupling with ice–ocean interactions is missing in our model yet, and Fürst et al. (2015) found that ocean warming caused additional mass loss of the GrIS in his projections applying a parameterization of ocean warming.

Our additional sea level rise for the year 2100 due to elevation SMB feedback is somewhat higher than that by Le clec’h et al. (2017), who used the regional model MAR actively coupled to an ice sheet model for their simulations. In contrast, Edwards et al. (2014) found an even smaller impact of this feedback than Le clec’h et al. (2017), possibly due to an underestimation  
10 of its spatial dependence in Edward’s parameterization. As demonstrated to be important by Le clec’h et al. (2017) with fully interactive two-way coupling, this feedback deserves a detailed inspection in the future.

Our presented projections for the GrIS contribution to global sea level rise in the 21st century (1.9–13.0 cm) are consistent with previous publications. However, they do not account for the dynamic response of Greenland outlet glaciers to ocean warming and increase of subglacial discharge. This effect will be account for in a forthcoming paper. We also intend to couple  
15 the 3-D ice sheet model SICOPOLIS with the 1-D model for many outlet glaciers.

## 7 Conclusions

We introduced the coupled Greenland glacial system model IGLOO 1.0 designed to describe the most important parts of the Greenland glacial system: the ice sheet, the subglacial hydrological system, the outlet glaciers and the ice-ocean interaction in the Greenland fjords. Full coupling between the ice sheet model and the model of subglacial water HYDRO has been  
20 accomplished, while the coupling between HYDRO and the meltwater plume works only off-line yet.

The applicability of the hybrid mode of the ice sheet model SICOPOLIS 3.3 to the Greenland ice sheet was demonstrated. It showed that the model performs reasonably well, as the simulated velocity field compared well with observations, including the two major outlet glaciers Helheim Glacier and Kangerdlugssuaq Glacier and the Jakobshavn Isbræ ice stream. Further, for simulating optimal velocities, it is reasonable that the sliding coefficient for the model in hybrid mode is larger than that for  
25 the SIA model, as lateral strain partly compensates the effect of basal drag.

As initialization, we used a relaxation method similar to Aschwanden et al. (2013), but with a somewhat higher relaxation constant of 100 years. For this choice of the relaxation constant, we varied it systematically and investigated the resulting model behaviour by inspecting the RMS error in surface elevation as well as the difference between total simulated SMB and total SMB from the MAR regional climate model. It showed that, for a relaxation constant of 100 years, the deviation of our  
30 simulated total SMB from the MAR SMB is about zero, while – at the same time – the RMS of the simulated error in surface elevation stays reasonably small. Additionally, we showed that medium-value relaxation times lead to smooth 2-D fields of the implied SMB, while for too small relaxation times the fields become rather noisy, and for too large relaxation times regional deviations of the simulated elevation from the observed one become relatively large.



Furthermore, we performed projections of the contribution of the GrIS to sea level rise until the year 2300 with hybrid ice dynamics forced by SMB anomalies from the MAR regional model. For the RCP 4.5 and 8.5 scenarios generated by MAR, three CMIP5 GCMs with different climate sensitivity were applied. Altogether, our projected GrIS sea level contribution for the year 2100 obtained with elevation SMB feedback ranges from 1.9 to 13.0 cm, and for the year 2300 from 3.5 to 76.4 cm. The elevation SMB feedback showed to be important. Generally, its impact increases in the long run with decreasing surface elevation (see Table 2).

Moreover, we demonstrated the importance of the different factors determining the increase of the melt rate of Greenland outlet glaciers under the extreme RCP 8.5 scenario, using Store and Helheim Glaciers as examples. It showed that the knowledge of near-terminus temperature and subglacial discharge in the fjord are both about equally important to determine the future melt of these two outlet glaciers. This underlines the importance of our approach with the Greenland system model IGLOO 1.0.

*Code and data availability.* SICOPOLIS is available at [www.sicopolis.net](http://www.sicopolis.net). The HYDRO module is not included in the repository yet. MAR data used as basis for our forcing is available at <ftp://ftp.climato.be/fettweis/MARv3.5/Greenland/>.

### Appendix A: Mass conservating scheme for ice thickness evolution

We included a new numerical scheme into SICOPOLIS 3.3, which discretizes the advection term of the ice thickness equation by a strictly mass-conserving scheme in an upwind flux form:

$$A = \frac{(\bar{v}_x(i+1/2, j)H_x^+ - \bar{v}_x(i-1/2, j)H_x^-)\Delta y + (\bar{v}_y(i, j+1/2)H_y^+ - \bar{v}_y(i, j-1/2)H_y^-)\Delta x}{\Delta x \Delta y}, \quad (\text{A1})$$

where  $A$  is the advection term and  $\bar{v}_x$ ,  $\bar{v}_y$  are the  $x$ - and  $y$ -components of the depth averaged velocity, respectively. Further,  $\Delta x$  and  $\Delta y$  are the horizontal spacings. The upwind coefficients read:

$$H_x^- = \begin{cases} H(i-1, j), & \bar{v}_x(i-1/2, j) \geq 0, \\ H(i, j), & \bar{v}_x(i-1/2, j) < 0, \end{cases} \quad H_x^+ = \begin{cases} H(i, j), & \bar{v}_x(i+1/2, j) \geq 0, \\ H(i+1, j), & \bar{v}_x(i+1/2, j) < 0, \end{cases}$$

$$H_y^- = \begin{cases} H(i, j-1), & \bar{v}_y(i, j-1/2) \geq 0, \\ H(i, j), & \bar{v}_y(i, j-1/2) < 0, \end{cases} \quad H_y^+ = \begin{cases} H(i, j), & \bar{v}_y(i, j+1/2) \geq 0, \\ H(i, j+1), & \bar{v}_y(i, j+1/2) < 0, \end{cases}$$

with the ice thickness  $H$ . The pairs  $(i, j)$ ,  $(i+1/2, j)$  etc. indicate the indices of the staggered Arakawa C grid.

### Appendix B: Adapting MAR data for the future simulations

One element of our initialization method (see Section 3) is the prevention of a model shock (Aschwanden et al., 2013) when we start the projections from the palaeo-spin-up and switch from fixed domain to free surface. Starting the free-surface simulations



as early as possible is preferable in order to give the model the chance to recover from possible perturbations at the beginning. While the MIROC5 model provides data starting at the year 1900, the CanESM2 and NorESM1 models start later in time at 1950. For the latter two models, we randomly reshuffled the horizontal time slices (annual mean of surface temperature, SMB and monthly surface runoff) from the years 1950–1999 back in time to the years 1900–1949. This yields forcing data for the 5 years 1900–2100 for all three CMIP5 models.

As ice sheets react on longer timescales, we needed longer scenarios and opted to prolong the scenario data until the year 2300. However, for the years 2101–2300, there are no direct scenario data available from MAR for any of the three used CMIP5 models. In particular, for RCP 8.5, we have the problem to choose a favourable sampling interval for the horizontal time slices. If we choose the sampling interval too short, there are not enough time slices to be assigned to the time beyond 2100, and 10 there is almost no variability. If we choose the interval too long, there is an overestimation of variability during the artificially prolonged interval 2101–2300 due to the already present climate-warming trend in the MAR RCP 8.5 forcing for the years towards the year 2100. This problem is particularly prevalent for the anomaly in SMB. A sampling length of 10 years (years 2091–2100) is a good choice. Over this sampling interval, the horizontal time slices are repeatedly and randomly reshuffled forward in time to the years 2101–2300. We found that there still was an overestimation of variability in the prolonged data.

15 We circumvented this overestimation of variability for (and only for) the RCP 8.5 scenarios by computing over the sampling interval the temporal average, the maximum and the minimum of the anomaly of the total SMB,  $\Delta M_{\text{tot}}^{\text{ave}}$ ,  $\Delta M_{\text{tot}}^{\text{min}}$  and  $\Delta M_{\text{tot}}^{\text{max}}$ , respectively. Then, we apply the condition

$$\Delta M_{\text{tot}} > \Delta M_{\text{tot}}^{\text{ave}} + 0.3 \cdot (\Delta M_{\text{tot}}^{\text{max}} - \Delta M_{\text{tot}}^{\text{min}}) / 2 \quad (\text{B1})$$

in order to exclude time slices with too positive total SMB anomaly. In fact, we consider 2-D fields where  $\Delta M$  totals are 20 below its average, while we consider only about the first 1/3 where  $\Delta M$  totals are above its average. Note that the totals of anomalies of surface mass balance are negative in these scenarios.

*Competing interests.* The authors declare no competing interests.

*Acknowledgements.* We are grateful to Fiamma Straneo and Dustin Carroll for providing us with temperature and salinity profiles of Helheim glacier. We are also grateful to Xavier Fettweis for hosting the website with the MAR data. Further, we would like to thank Ciarion Linstead 25 for technical support with library installation. J. B., R. C. and S. B. were funded by the Leibniz Association grant SAW-2014-PIK-1. M. R. was supported by the Helmholtz Alliance Climate Initiative (REKLIM). M. W. is supported by the Bundesministerium für Bildung und Forschung (BMBF) grants PalMod-2.1 and PalMod-2.2. R. C. is funded by the Bundesministerium für Bildung und Forschung (BMBF) grants PalMod-1.1 and PalMod-1.3. R. G. was supported by Japan Society for the Promotion of Science (JSPS) KAKENHI grant numbers 16H02224 and 17H06104, and by the Arctic Challenge for Sustainability (ArCS) project of the Japanese Ministry of Education, Culture, 30 Sports, Science and Technology (MEXT).



## References

- Arakawa, A. and Lamb, V. R.: Computational design of the basic dynamical processes of the UCLA general circulation model, in: *Methods in Computational Physics* Vol. 17, edited by Chang, J., pp. 173–265, Academic Press, New York, NY, USA, 1977.
- Aschwanden, A., Aðalgeirsdóttir, G., and Khroulev, C.: Hindcasting to measure ice sheet model sensitivity to initial states, *The Cryosphere*, 7, 1083–1093, doi:10.5194/tc-7-1083-2013, <https://www.the-cryosphere.net/7/1083/2013/>, 2013.
- Aschwanden, A., Fahnestock, M. A., and Truffer, M.: Complex Greenland outlet glacier flow captured, *Nat. Commun.*, 7, 10524, doi:10.1038/ncomms10524, 2016.
- Bales, R. C., Guo, Q., Shen, D., McConnell, J. R., Du, G., Burkhart, J. F., Spikes, V. B., Hanna, E., and Cappelen, J.: Annual accumulation for Greenland updated using ice core data developed during 2000–2006 and analysis of daily coastal meteorological data, *J. Geophys. Res.*, 114, D06 116, doi:10.1029/2008JD011208, 2009.
- Bamber, J. L., Griggs, J. A., Hurkmans, R. T. W. L., Dowdeswell, J. A., Gogineni, S. P., Howat, I., Mouginot, J., Paden, J., Palmer, S., Rignot, E., and Steinhage, D.: A new bed elevation dataset for Greenland, *The Cryosphere*, 7, 499–510, doi:10.5194/tc-7-499-2013, 2013.
- Barnes, R., Lehman, C., and Mulla, D.: Priority-flood: An optimal depression-filling and watershed-labeling algorithm for digital elevation models, *Computers & Geosciences*, 62, 117–127, doi:10.1016/j.cageo.2013.04.024, 2014.
- Beckmann, J., Perrette, M., and Ganopolski, A.: Submarine melt parameterization for a Greenland glacial system model, *The Cryosphere*, nn, nn, doi:nn, 2017.
- Bernales, J., Rogozhina, I., Greve, R., and Thomas, M.: Comparison of hybrid schemes for the combination of shallow approximations in numerical simulations of the Antarctic Ice Sheet, *The Cryosphere*, 11, 247–265, doi:10.5194/tc-11-247-2017, 2017.
- Box, J. E. and Colgan, W.: Greenland ice sheet mass balance reconstruction. Part III: marine ice loss and total mass balance (1840–2010), *J. Climate*, doi:10.1175/JCLI-D-12-00546.1, 2013.
- Box, J. E., Yang, L., Bromwich, D. H., and Bai, L.-S.: Greenland ice sheet surface air temperature variability: 1840–2007, *Journal of Climate*, 22, 4029–4049, doi:10.1175/2009JCLI2816.1, <https://doi.org/10.1175/2009JCLI2816.1>, 2009.
- Bueler, E. and Brown, J.: Shallow shelf approximation as a “sliding law” in a thermomechanically coupled ice sheet model, *J. Geophys. Res.*, 114, F03 008, doi:10.1029/2008JF001179, 2009.
- Calov, R. and Hutter, K.: The thermomechanical response of the Greenland ice sheet to various climate scenarios, *Clim. Dynam.*, 12, 243–260, 1996.
- Calov, R., Robinson, A., Perrette, M., and Ganopolski, A.: Simulating the Greenland ice sheet under present-day and palaeo constraints including a new discharge parameterization, *The Cryosphere*, 9, 179–196, doi:10.5194/tc-9-179-2015, 2015.
- Carroll, D., Sutherland, D. A., Shroyer, E. L., D., N. J., Catania, G. A., and A., S. L.: Modeling turbulent subglacial meltwater plumes: Implications for fjord-scale buoyancy-driven circulation, *Journal of Physical Oceanography*, 45, 2169–2185, doi:10.1175/JPO-D-15-0033.1, <https://doi.org/10.1175/JPO-D-15-0033.1>, 2015.
- Carroll, D., Sutherland, D. A., Hudson, B., Moon, T., Catania, G. A., Shroyer, E. L., Nash, J. D., Bartholomaeus, T. C., Felikson, D., Stearns, L. A., Noël, B. P. Y., and van den Broeke, M. R.: The impact of glacier geometry on meltwater plume structure and submarine melt in Greenland fjords, *Geophysical Research Letters*, pp. 1–10, doi:10.1002/2016GL070170, <http://doi.wiley.com/10.1002/2016GL070170>, 2016.



- Chauché, N., Hubbard, A., Gascard, J. C., Box, J. E., Bates, R., Koppes, M., Sole, A., Christoffersen, P., and Patton, H.: Ice-ocean interaction and calving front morphology at two west Greenland tidewater outlet glaciers, *Cryosphere*, 8, 1457–1468, doi:10.5194/tc-8-1457-2014, 2014.
- Church, J., Clark, P. U., Cazenave, A., Gregory, J. M., Jevrejeva, S., Levermann, A., Merrifield, M. A., Milne, G. A., Nerem, R. S., Nunn, P. D., Payne, A. J., Pfeffer, W. T., Stammer, D., and Unnikrishnan, A. S.: Sea Level Change, in: *Climate Change 2013: The Physical Science Basis. Contribution of Working Group I to the Fifth Assessment Report of the Intergovernmental Panel on Climate Change*, edited by Stocker, T. F., Qin, D., Plattner, G.-K., Tignor, M., Allen, S. K., Boschung, J., Nauels, A., Xia, Y., Bex, V., and Midgley, P. M., pp. 1137–1216, Cambridge University Press, Cambridge, United Kingdom and New York, NY, USA, 2013.
- 5 Claussen, M., Mysak, L. A., Weaver, A. J., Crucifix, M., Fichet, T., Loutre, M.-F., Weber, S. L., Alcamo, J., Alexeev, V. A., Berger, A., Calov, R., Ganopolski, A., Goosse, H., Lohman, G., Lunkeit, F., Mokhov, I. I., Petoukhov, V., Stone, P., and Wang, Z.: Earth system models of intermediate complexity: Closing the gap in the spectrum of climate system models, *Clim. Dyn.*, 18, 579–586, doi:10.1007/s00382-001-0200-1, 2002.
- Collins, M., Knutti, R., J. Arblaster, J., Dufresne, J.-L., Fichet, T., Friedlingstein, P., Gao, X., Gutowski, W. J., Johns, T., Krinner, G., Shongwe, M., Tebaldi, C., Weaver, A. J., and Wehner, M.: Long-term Climate Change: Projections, Commitments and Irreversibility, in: *Climate Change 2013: The Physical Science Basis. Contribution of Working Group I to the Fifth Assessment Report of the Intergovernmental Panel on Climate Change*, edited by Stocker, T. F., Qin, D., Plattner, G.-K., Tignor, M., Allen, S. K., Boschung, J., Nauels, A., Xia, Y., Bex, V., and Midgley, P. M., pp. 1029–1136, Cambridge University Press, Cambridge, United Kingdom and New York, NY, USA, 2013.
- 15 Cowton, T., Slater, D., Sole, A., Goldberg, D., and Nienow, P.: Modeling the impact of glacial runoff on fjord circulation and submarine melt rate using a new subgrid-scale parameterization for glacial plumes, *Journal of Geophysical Research: Oceans*, pp. 796–812, doi:10.1002/2014JC010324, <http://doi.wiley.com/10.1002/2014JC010324>, 2015.
- Edwards, T. L., Fettweis, X., Gagliardini, O., Gillet-Chaulet, F., Goelzer, H., Gregory, J. M., Hoffman, M., Huybrechts, P., Payne, A. J., Perego, M., Price, S., A., Q., and Ritz, C.: Effect of uncertainty in surface mass balance–elevation feedback on projections of the future sea level contribution of the Greenland ice sheet, *The Cryosphere*, 8, 195–208, doi:10.5194/tc-8-195-2014, 2014.
- 25 Enderlin, E. M., Howat, I. M., Jeong, S., Noh, M.-J., van Angelen, J. H., and van den Broeke, M. R.: An improved mass budget for the Greenland ice sheet, *Geophys. Res. Lett.*, 41, 866–872, doi:10.1002/2013GL059010, 2014.
- Ettema, J., van den Broeke, M. R., van Meijgaard, E., van de Berg, W. J., Bamber, J. L., Box, J. E., and Bales, R. C.: Higher surface mass balance of the Greenland ice sheet revealed by high-resolution climate modeling, *Geophys. Res. Lett.*, 36, L12501, doi:10.1029/2009GL038110, 2009.
- 30 Fettweis, X., Franco, B., Tedesco, M., van Angelen, J. H., , Lenaerts, J. T. M., van den Broeke, M. R., and Gallée, H.: Estimating the Greenland ice sheet surface mass balance contribution to future sea level rise using the regional atmospheric climate model MAR, *The Cryosphere*, 7, 469–489, doi:10.5194/tc-7-469-2013, 2013.
- Fürst, J. J., Goelzer, H., and Huybrechts, P.: Effect of higher-order stress gradients on the centennial mass evolution of the Greenland ice sheet, *The Cryosphere*, 7, 183–199, doi:10.5194/tc-7-183-2013, 2013.
- 35 Fürst, J. J., Goelzer, H., and Huybrechts, P.: Ice-dynamic projections of the Greenland ice sheet in response to atmospheric and oceanic warming, *The Cryosphere*, 9, 1039–1062, doi:10.5194/tc-9-1039-2015, 2015.
- Ganopolski, A. and Calov, R.: The role of orbital forcing, carbon dioxide and regolith in 100 kyr glacial cycles, *Clim. Past*, 7, 1415–1425, doi:10.5194/cp-7-1415-2011, 2011.



- Gillet-Chaulet, F., Gagliardini, O., Seddik, H., Nodet, M., Durand, G., Ritz, C., Zwinger, T., Greve, R., and Vaughan, D. G.: Greenland ice sheet contribution to sea-level rise from a new-generation ice-sheet model, *The Cryosphere*, 6, 1561–1576, doi:10.5194/tc-6-1561-2012, <https://www.the-cryosphere.net/6/1561/2012/>, 2012.
- Goelzer, H., Huybrechts, P., Fürst, J. J., Nick, F. M., Andersen, M. L., Edwards, T. L., Fettweis, X., Payne, A. J., and Shannon, S.: Sensitivity of Greenland ice sheet projections to model formulations, *J. Glaciol.*, 59, 733–549, doi:10.3189/2013JoG12J182, 2013.
- Gregory, J. and Huybrechts, P.: Ice-sheet contributions to future sea-level change, *Philos. Trans. R. Soc. Lond. A*, 364, 1709—1731, doi:10.1098/rsta.2006.1796, 2006.
- Greve, R.: Thermomechanisches Verhalten polythermer Eisschilde – Theorie, Analytik, Numerik, Doctoral thesis, Department of Mechanics, Darmstadt University of Technology, Germany, *Berichte aus der Geowissenschaft*, Shaker Verlag, Aachen, Germany, 1995.
- Greve, R.: Application of a polythermal three-dimensional ice sheet model to the Greenland ice sheet: Response to steady-state and transient climate scenarios, *J. Climate*, 10, 901–918, doi:10.1175/1520-0442(1997)010<0901:AOAPTD>2.0.CO;2, 1997.
- Greve, R.: On the response of the Greenland ice sheet to greenhouse climate change, *Climatic Change*, 46, 289–303, 2000.
- Greve, R. and Blatter, H.: *Dynamics of Ice Sheets and Glaciers*, Springer, Berlin, Germany etc., doi:10.1007/978-3-642-03415-2, 2009.
- Greve, R. and Blatter, H.: Comparison of thermodynamics solvers in the polythermal ice sheet model SICOPOLIS, *Polar Science*, 10, 11–23, doi:10.1016/j.polar.2015.12.004, 2016.
- Greve, R., Calov, R., and Herzfeld, U. C.: Projecting the response of the Greenland ice sheet to future climate change with the ice sheet model SICOPOLIS, *Low Temperature Science*, 75, 117–129, doi:10.14943/lowtemsci.75.117, 2017.
- Gudlaugsson, E., Humbert, A., Andreassen, K., Clason, C. C., Kleiner, T., and Beyer, S.: Eurasian ice-sheet dynamics and sensitivity to subglacial hydrology, *Journal of Glaciology*, 63, 556–564, doi:10.1017/jog.2017.21, 2017.
- Helm, V., Humbert, A., and Miller, H.: Elevation and elevation change of Greenland and Antarctica derived from CryoSat-2, *The Cryosphere*, 8, 1539–1559, doi:10.5194/tc-8-1539-2014, <https://www.the-cryosphere.net/8/1539/2014/>, 2014.
- Helsen, M. M., van de Wal, R. S. W., van den Broeke, M. R., van de Berg, W. J., and Oerlemans, J.: Coupling of climate models and ice sheet models by surface mass balance gradients: application to the Greenland Ice Sheet, *The Cryosphere*, 6, 255—272, doi:10.5194/tc-6-255-2012, 2012, 2012.
- Hindmarsh, R. C. A.: A numerical comparison of approximations to the Stokes equations used in ice sheet and glacier modeling, *Journal of Geophysical Research: Earth Surface*, 109, doi:10.1029/2003JF000065, <http://dx.doi.org/10.1029/2003JF000065>, f01012, 2004.
- Hindmarsh, R. C. A. and Le Meur, E.: Dynamical processes involved in the retreat of marine ice sheets, *J. Glaciol.*, 47, 271—282, 2001.
- Hubbard, A., Bradwell, T., Gollledge, N., Hall, A., Patton, H., Sugden, D., Cooper, R., and Stoker, M.: Dynamic cycles, ice streams and their impact on the extent, chronology and deglaciation of the British-Irish ice sheet, *Quaternary Science Reviews*, 28, 758–776, doi:<https://doi.org/10.1016/j.quascirev.2008.12.026>, <http://www.sciencedirect.com/science/article/pii/S0277379109000201>, 2009.
- Hutter, K.: *Theoretical Glaciology; Material Science of Ice and the Mechanics of Glaciers and Ice Sheets*, D. Reidel Publishing Company, Dordrecht, The Netherlands, 1983.
- Huybrechts, P. and de Wolde, J.: The dynamic response of the Antarctic and Greenland ice sheets to multiple-century climatic warming, *J. Climate*, 12, 2169–2188, doi:10.1175/1520-0442(1999)012<2169:TDR0TG>2.0.CO;2, 1999.
- Jackson, R. H., Straneo, F., and Sutherland, D. A.: Externally forced fluctuations in ocean temperature at Greenland glaciers in non-summer months, *Nature Geoscience*, 7, 503–508, doi:10.1038/ngeo2186, [http://www.nature.com/ngeo/journal/v7/n7/full/ngeo2186.html?WT.ec\\_id=NGEO-201407](http://www.nature.com/ngeo/journal/v7/n7/full/ngeo2186.html?WT.ec_id=NGEO-201407), 2014.



- Jackson, R. H., Shroyer, E. L., Nash, J. D., Sutherland, D. A., Carroll, D., Fried, M. J., Catania, G. A., Bartholomaeus, T. C., and Stearns, L. A.: Near-glacier surveying of a subglacial discharge plume: implications for plume parameterizations, *Geophysical Research Letters*, doi:10.1002/2017GL073602, <http://doi.wiley.com/10.1002/2017GL073602>, 2017.
- Jenkins, A.: Convection-Driven Melting near the Grounding Lines of Ice Shelves and Tidewater Glaciers, *Journal of Physical Oceanography*, 5 41, 2279–2294, doi:10.1175/JPO-D-11-03.1, <http://journals.ametsoc.org/doi/abs/10.1175/JPO-D-11-03.1>, 2011.
- Joughin, I., Smith, B. E., Howat, I. M., Scambos, T., and Moon, T.: Greenland flow variability from ice-sheet-wide velocity mapping, *J. Glaciol.*, 56, 415–430, 2010.
- Kleiner, T. and Humbert, A.: Numerical simulations of major ice streams in western Dronning Maud Land, Antarctica, under wet and dry basal conditions, *Journal of Glaciology*, 60, 215–232, doi:10.3189/2014JoG13J006, <http://www.igsoc.org/journal/60/220/t13J006.html>, 10 2014.
- Kusahara, K., Sato, T., Oka, A., Obase, T., Greve, R., Abe-Ouchi, A., and Hasumi, H.: Modelling the Antarctic marine cryosphere at the Last Glacial Maximum, *Annals of Glaciology*, 56, 425–435, doi:10.3189/2015AoG69A792, 2015.
- Le Brocq, A., Payne, A., Siegert, M., and Alley, R.: A subglacial water-flow model for West Antarctica, *Journal of Glaciology*, 55, 879–888, 2009.
- 15 Le Brocq, A. M., Payne, A. J., and Siegert, M. J.: West Antarctic balance calculations: impact of flux-routing algorithm, smoothing algorithm and topography, *Computers & geosciences*, 32, 1780–1795, 2006.
- Le clec’h, S., Fettweis, X., Quiquet, A., Dumas, C., Kageyama, M., Charbit, S., Wyard, C., and Ritz, C.: Assessment of the Greenland ice sheet – atmosphere feedbacks for the next century with a regional atmospheric model fully coupled to an ice sheet model, *The Cryosphere Discussions*, 2017, 1–31, doi:10.5194/tc-2017-230, <https://www.the-cryosphere-discuss.net/tc-2017-230/>, 2017.
- 20 Le Meur, E. and Huybrechts, P.: A comparison of different ways of dealing with isostasy: examples from modelling the Antarctic ice sheet during the last glacial cycle, *Annals of Glaciology*, 23, 309–317, 1996.
- Livingstone, S. J., Clark, C. D., Woodward, J., and Kingslake, J.: Potential subglacial lakes and meltwater drainage pathways beneath the Antarctic and Greenland ice sheets, *The Cryosphere*, 7, 1721–1740, 2013.
- Lliboutry, L. and Duval, P.: Various isotropic and anisotropic ices found in glaciers and polar ice caps and their corresponding rheologies., 25 *Ann. Geophys.*, 3, 207–224, 1985.
- MacAyeal, D. R.: Large-scale ice flow over a viscous basal sediment: theory and application to ice stream B, Antarctica, *Journal of Geophysical Research: Solid Earth*, 94, 4071–4087, 1989.
- MacGregor, J. A., Fahnestock, M. A., Catania, G. A., Aschwanden, A., Clow, G. D., Colgan, W. T., Gogineni, S. P., Morlighem, M., Nowicki, S. M. J., Paden, J. D., Price, S. F., and Seroussi, H.: A synthesis of the basal thermal state of the Greenland ice sheet, *J. Geophys. Res.*, 30 121, 1328–1350, doi:10.1002/2015JF003803, 2016.
- Morland, L. W.: Thermomechanical balances of ice sheet flows, *Geophysical and Astrophysical Fluid Dynamics*, 29, 237–266, 1984.
- Morland, L. W.: Unconfined ice-shelf flow, in: *Dynamics of the West Antarctic Ice Sheet*, edited by van der Veen, C. J. and Oerlemans, J., pp. 99–116, D. Reidel Publishing Company, Dordrecht, The Netherlands, 1987.
- Morlighem, M., Rignot, E., Mouginot, J., Seroussi, H., and Larour, E.: Deeply incised submarine glacial valleys beneath the Greenland ice sheet, *Nature Geosci*, 7, 418–422, doi:10.1038/ngeo2167, 2014.
- 35 Murray, T., Scharer, K., James, T. D., Dye, S. R., Hanna, E., Booth, A. D., Selmes, N., Luckman, A., Hughes, A. L. C., Cook, S., and Huybrechts, P.: Ocean regulation hypothesis for glacier dynamics in southeast Greenland and implications for ice sheet mass changes, *Journal of Geophysical Research: Earth Surface*, 115, doi:10.1029/2009JF001522, <http://dx.doi.org/10.1029/2009JF001522>, f03026, 2010.



- Nick, F. M., Vieli, A., Andersen, M. L., Joughin, I., Payne, A., Edwards, T. L., Pattyn, F., and van de Wal, R. S. W.: Future sea-level rise from Greenland's main outlet glaciers in a warming climate, *Nature*, 497, 235–238, <http://dx.doi.org/10.1038/nature12068>, 2013.
- Nienow, P. W., Sole, A. J., Slater, D. A., and Cowton, T. R.: Recent advances in our understanding of the role of meltwater in the Greenland ice sheet system, *Current Climate Change Reports*, pp. 330–344, doi:10.1007/s40641-017-0083-9, <http://link.springer.com/10.1007/s40641-017-0083-9>, 2017.
- 5 s40641-017-0083-9, 2017.
- O'Leary, M. and Christoffersen, P.: Calving on tidewater glaciers amplified by submarine frontal melting, *The Cryosphere*, 7, 119–128, doi:10.5194/tc-7-119-2013, <https://www.the-cryosphere.net/7/119/2013/>, 2013.
- Pattyn, F.: Sea-level response to melting of Antarctic ice shelves on multi-centennial timescales with the fast Elementary Thermomechanical Ice Sheet model (f.ETISH v1.0), *The Cryosphere*, 11, 1851–1878, doi:10.5194/tc-11-1851-2017, <https://www.the-cryosphere.net/11/1851/> 2017, 2017.
- 10 2017, 2017.
- Peano, D., Colleoni, F., Quiquet, A., and Masina, S.: Ice flux evolution in fast flowing areas of the Greenland ice sheet over the 20th and 21st centuries, *J. Glaciol.*, 63, 499–513, doi:10.1017/jog.2017.12, 2017.
- Pollard, D. and DeConto, R. M.: A coupled ice-sheet/ice-shelf/sediment model applied to a marine-margin flowline: forced and unforced variations, in: *Glacial Sedimentary Processes and Products*, edited by Hambrey, M. J., Christoffersen, P., Glasser, N. F., and Hubbard, B., pp. 37–52, Blackwell Publishing Ltd., Oxford, UK., doi:10.1002/9781444304435.ch4, 2007.
- 15 pp. 37–52, Blackwell Publishing Ltd., Oxford, UK., doi:10.1002/9781444304435.ch4, 2007.
- Pollard, D. and DeConto, R. M.: Description of a hybrid ice sheet-shelf model, and application to Antarctica, *Geoscientific Model Development*, 5, 1273–1295, doi:10.5194/gmd-5-1273-2012, <https://www.geosci-model-dev.net/5/1273/2012/>, 2012.
- Price, S. F., Payne, A. J., Howat, I., and Smith, B. E.: Committed sea-level rise for the next century from Greenland ice sheet dynamics during the past decade, *PNAS*, 108, 8978–8983, doi:www.pnas.org/cgi/doi/10.1073/pnas.1017313108, 2011.
- 20 Purucker, M.: personal communication with Ralf Greve, accessible via [www.sicopolis.net](http://www.sicopolis.net), 2012.
- Rietbroek, R., Brunnabend, S.-E., Kusche, J., Schröter, J., and Dahle, C.: Revisiting the contemporary sea-level budget on global and regional scales, *Proceedings of the National Academy of Sciences*, 113, 1504–1509, doi:10.1073/pnas.1519132113, <http://www.pnas.org/content/113/6/1504.abstract>, 2016.
- Rignot, E. and Mouginot, J.: Ice flow in Greenland for the International Polar Year 2008-2009, *Geophys. Res. Lett.*, 39, L11 501, doi:10.1029/2012GL051634, 2012.
- 25 doi:10.1029/2012GL051634, 2012.
- Rignot, E., Fenty, I., Xu, Y., Cai, C., and Kemp, C.: Undercutting of marine-terminating glaciers in West Greenland, *Geophysical Research Letters*, 42, 5909–5917, doi:10.1002/2015GL064236, 2015.
- Ritz, C., Rommelaere, V., and Dumas, C.: Modeling the evolution of Antarctic ice sheet over the last 420,000 years: Implications for altitude changes in the Vostok region, *Journal of Geophysical Research: Atmospheres*, 106, 31 943–31 964, doi:10.1029/2001JD900232, <http://dx.doi.org/10.1029/2001JD900232>, 2001.
- 30 <http://dx.doi.org/10.1029/2001JD900232>, 2001.
- Robinson, A., Calov, R., and Ganopolski, A.: Greenland ice sheet model parameters constrained using simulations of the Eemian interglacial, *Clim. Past*, 7, 381–396, doi:10.5194/cp-7-381-2011, 2011.
- Robinson, A., Calov, R., and Ganopolski, A.: Multistability and critical thresholds of the Greenland ice sheet, *Nature Climate Change*, 2, 429–432, doi:10.1038/NCLIMATE1449, 2012.
- 35 Rogozhina, I., Petrunin, A. G., Vaughan, A. P. M., Steinberger, B., Johnson, J. V., Kaban, M. K., Calov, R., Rickers, F., Thomas, M., and Koulakov, I.: Melting at the base of the Greenland Ice Sheet explained by Iceland hotspot history, *Nat Geosci*, 9, 366–369, doi:10.1038/NCEO2689, <http://dx.doi.org/10.1038/ngeo2689>, 2016.



- Saito, F., Abe-Ouchi, A., Takahashi, K., and Blatter, H.: SeaRISE experiments revisited: potential sources of spread in multi-model projections of the Greenland ice sheet, *The Cryosphere*, 10, 43–63, doi:10.5194/tc-10-43-2016, <https://www.the-cryosphere.net/10/43/2016/>, 2016.
- Sciascia, R., Straneo, F., Cenedese, C., and Heimbach, P.: Seasonal variability of submarine melt rate and circulation in an East Greenland fjord, *Journal of Geophysical Research: Oceans*, 118, 2492–2506, doi:10.1002/jgrc.20142, <http://doi.wiley.com/10.1002/jgrc.20142>, 2013.
- 5 Seddik, H., Greve, R., Zwinger, T., Gillet-Chaulet, F., and Gagliardini, O.: Simulations of the Greenland ice sheet 100 years into the future with the full Stokes model Elmer/Ice, *J. Glaciol.*, 58, 427–440, doi:10.3189/2012JoG11J177, 2012.
- Shreve, R.: Movement of water in glaciers, *Journal of Glaciology*, 11, 205–214, 1972.
- Slater, D., Nienow, P., Sole, A., Cowton, T., Mottram, R., Langen, P., and Mair, D.: Spatially distributed runoff at the grounding line of a large Greenlandic tidewater glacier inferred from plume modelling, *Journal of Glaciology*, pp. 1–15, doi:10.1017/jog.2016.139, 2017.
- 10 Slater, D. A., Nienow, P. W., Cowton, T. R., Goldberg, D. N., and Sole, A. J.: Effect of near-terminus subglacial hydrology on tidewater glacier submarine melt rates, *Geophysical Research Letters*, 42, 2861–2868, doi:10.1002/2014GL062494, 2015.
- Stone, E., Lunt, D. J., Annan, J. D., and Hargreaves, J. C.: Quantification of the Greenland ice sheet contribution to Last Interglacial sea level rise, *Clim. Past*, 9, 621–639, doi:10.5194/cp-9-621-2013, 2013.
- 15 Straneo, F., Curry, R. G., Sutherland, D. A., Hamilton, G. S., Cenedese, C., Våge, K., and Stearns, L. A.: Impact of fjord dynamics and glacial runoff on the circulation near Helheim Glacier, *Nature Geoscience*, 4, 322–327, doi:10.1038/ngeo1109, <http://www.nature.com/doi/10.1038/ngeo1109>, 2011.
- Straneo, F., Sutherland, D. A., Holland, D., Gladish, C., Hamilton, G. S., Johnson, H. L., Rignot, E., Xu, Y., and Koppes, M.: Characteristics of ocean waters reaching Greenland’s glaciers, *Annals of Glaciology*, 53, 202–210, doi:10.3189/2012AoG60A059, 2012.
- 20 Straneo, F., Hamilton, G. S., Stearns, L. A., and Sutherland, D. A.: Connecting the Greenland ice sheet and the ocean: A case study of Helheim Glacier and Sermilik Fjord, *Oceanography*, 29, <https://doi.org/10.5670/oceanog.2016.97>, 2016.
- Sutherland, D. A. and Straneo, F.: Estimating ocean heat transports and submarine melt rates in Sermilik Fjord, Greenland, using lowered acoustic doppler current profiler (LADCP) velocity profiles, *Annals of Glaciology*, 53, 50–58, doi:10.3189/2012AoG60A050, 2012.
- Vallelonga, P., Christianson, K., Alley, R. B., Anandakrishnan, S., Christian, J. E. M., Dahl-Jensen, D., Gkinis, V., Holme, C., Jacobel, R. W., Karlsson, N. B., Keisling, B. A., Kipfstuhl, S., Kjær, H. A., Kristensen, M. E. L., Muto, A., Peters, L. E., Popp, T., Riverman, K. L., Svensson, A. M., Tibuleac, C., Vinther, B. M., Weng, Y., and Winstrup, M.: Initial results from geophysical surveys and shallow coring of the Northeast Greenland Ice Stream (NEGIS), *The Cryosphere*, 8, 1275–1287, doi:10.5194/tc-8-1275-2014, <https://www.the-cryosphere.net/8/1275/2014/>, 2014.
- van Angelen, J. H., Lenaerts, J. T. M., Lhermitte, S., Fettweis, X., Kuipers Munneke, P., van den Broeke, M. R., and van Meijgaard, E.: Sensitivity of Greenland Ice Sheet surface mass balance to surface albedo parameterization: a study with a regional climate model, *The Cryosphere Discussions*, 6, 1531–1562, doi:10.5194/tcd-6-1531-2012, <http://www.the-cryosphere-discuss.net/6/1531/2012/>, 2012.
- 30 van den Broeke, M. R., Enderlin, E. M., Howat, I. M., Kuipers Munneke, P., Noël, B. P. Y., van de Berg, W. J., van Meijgaard, E., and Wouters, B.: On the recent contribution of the Greenland ice sheet to sea level change, *The Cryosphere*, 10, 1933–1946, doi:10.5194/tc-10-1933-2016, <https://www.the-cryosphere.net/10/1933/2016/>, 2016.
- 35 Velicogna, I. and Wahr, J.: Greenland mass balance from GRACE, *Geophysical Research Letters*, 32, doi:10.1029/2005GL023955, <http://dx.doi.org/10.1029/2005GL023955>, 118505, 2005.



- Vizcaino, M., Mikolajewicz, U., Ziemen, F., Rodehacke, C. B., Greve, R., and van den Broeke, M. R.: Coupled simulations of Greenland Ice Sheet and climate change up to A.D. 2300, *Geophysical Research Letters*, 42, 3927–3935, doi:10.1002/2014GL061142, <http://dx.doi.org/10.1002/2014GL061142>, 2014GL061142, 2015.
- Weertman, J.: Effect of a Basal Water Layer on the Dimensions of Ice Sheets, *Journal of Glaciology*, 6, 191–207, doi:10.1017/S0022143000019213, 1966.
- 5 Weertman, J.: General theory of water flow at the base of a glacier or ice sheet, *Reviews of Geophysics*, 10, 287–333, doi:10.1029/RG010i001p00287, <http://dx.doi.org/10.1029/RG010i001p00287>, 1972.
- Winkelmann, R., Martin, M. A., Haseloff, M., Albrecht, T., Bueler, E., Khroulev, C., and Levermann, A.: The Potsdam Parallel Ice Sheet Model (PISM-PIK) – Part 1: Model description, *The Cryosphere*, 5, 715–726, doi:10.5194/tc-5-715-2011, <https://www.the-cryosphere.net/5/715/2011/>, 2011.
- 10 Xu, Y., Rignot, E., Fenty, I., Menemenlis, D., and Flexas, M. M.: Subaqueous melting of Store Glacier, west Greenland from three-dimensional, high-resolution numerical modeling and ocean observations, *Geophysical Research Letters*, 40, 4648–4653, doi:10.1002/grl.50825, <http://doi.wiley.com/10.1002/grl.50825>, 2013.
- Yin, J., Overpeck, J. T., Griffies, S. M., Hu, A., Russell, J. L., and Stouffer, R. J.: Different magnitudes of projected subsurface ocean warming around Greenland and Antarctica, *Nature Geoscience*, 4, 524–528, doi:10.1038/ngeo1189, <http://www.nature.com/doifinder/10.1038/ngeo1189>, 2011.
- 15



## Tables

**Table 1.** Abbreviations in Fig. 1.

Abbreviations	Physical meaning
$z_0$	Observed present-day elevation of GrIS
$z$	Simulated elevation
$\Delta T_{\text{GRIP}}$	Reconstruction of temperature anomaly from GRIP ice core
$\Delta T_s$	Anomaly of surface temperature simulated by MAR
$\Delta M$	Anomaly of surface mass balance simulated by MAR
$\Delta R$	Anomaly of runoff simulated by MAR
$T_s$	Surface temperature
$M$	Surface mass balance
$R$	Surface runoff
$Q$	Subglacial discharge into the given fjord
$B$	Bottom melt simulated by SICOPOLIS
$W$	Thickness of basal water layer
$T$	Ocean temperature (function of depth)
$S$	Ocean salinity (function of depth)

**Table 2.** Simulated GrIS contribution to sea level rise for the years 2100 and 2300 in cm. Columns specify the different GCMs used by MAR. Rows list the RCP scenarios used by the MAR GCMs and whether we excluded or included the elevation SMB feedback  $\partial M/\partial z$  in our simulation.

MAR GCM	Year 2100 [cm]				Year 2300 [cm]			
	RCP 4.5		RCP 8.5		RCP 4.5		RCP 8.5	
$\partial M/\partial z$	off	on	off	on	off	on	off	on
NorESM1	1.5	1.9	4.0	4.6	1.8	3.5	18.8	25.5
MIROC5	3.7	4.3	7.7	8.8	8.5	10.8	33.7	46.3
CanESM2	4.6	5.6	11.3	13.0	11.2	17.1	54.6	76.4



Figures

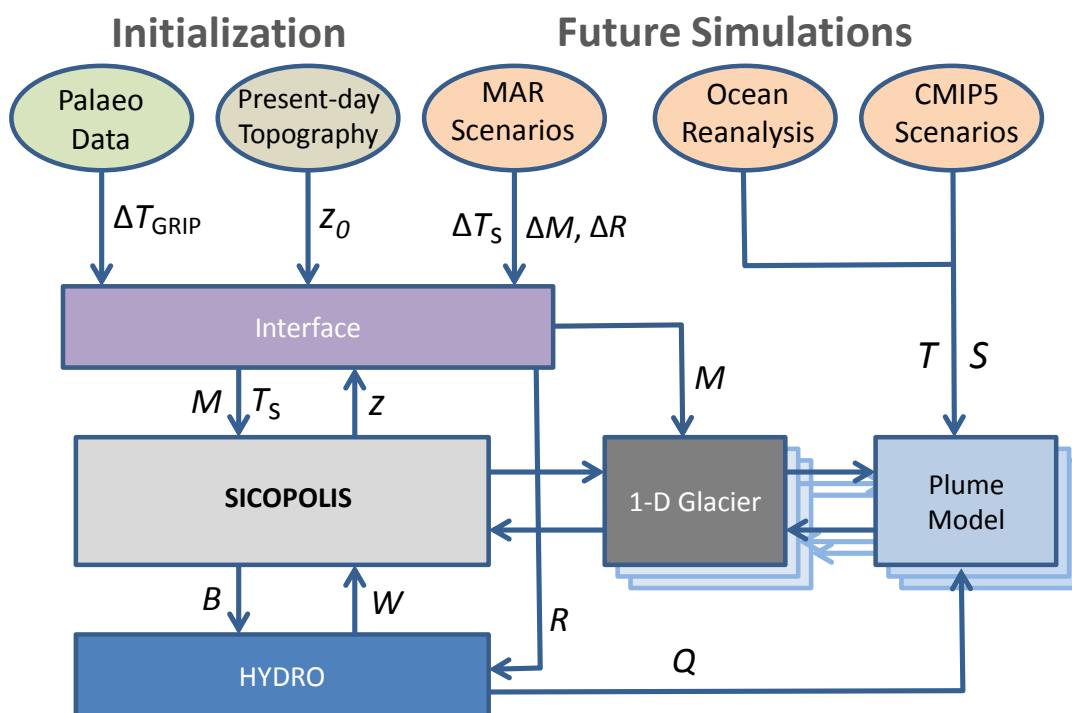


**Figure 1.** Flow diagram of the model IGLOO and the interaction between its components. The 1-D outlet glacier and plume models are generic models, i. e. they can be applied to each outlet glacier of the Greenland ice sheet. Abbreviations are explained in Table 1.

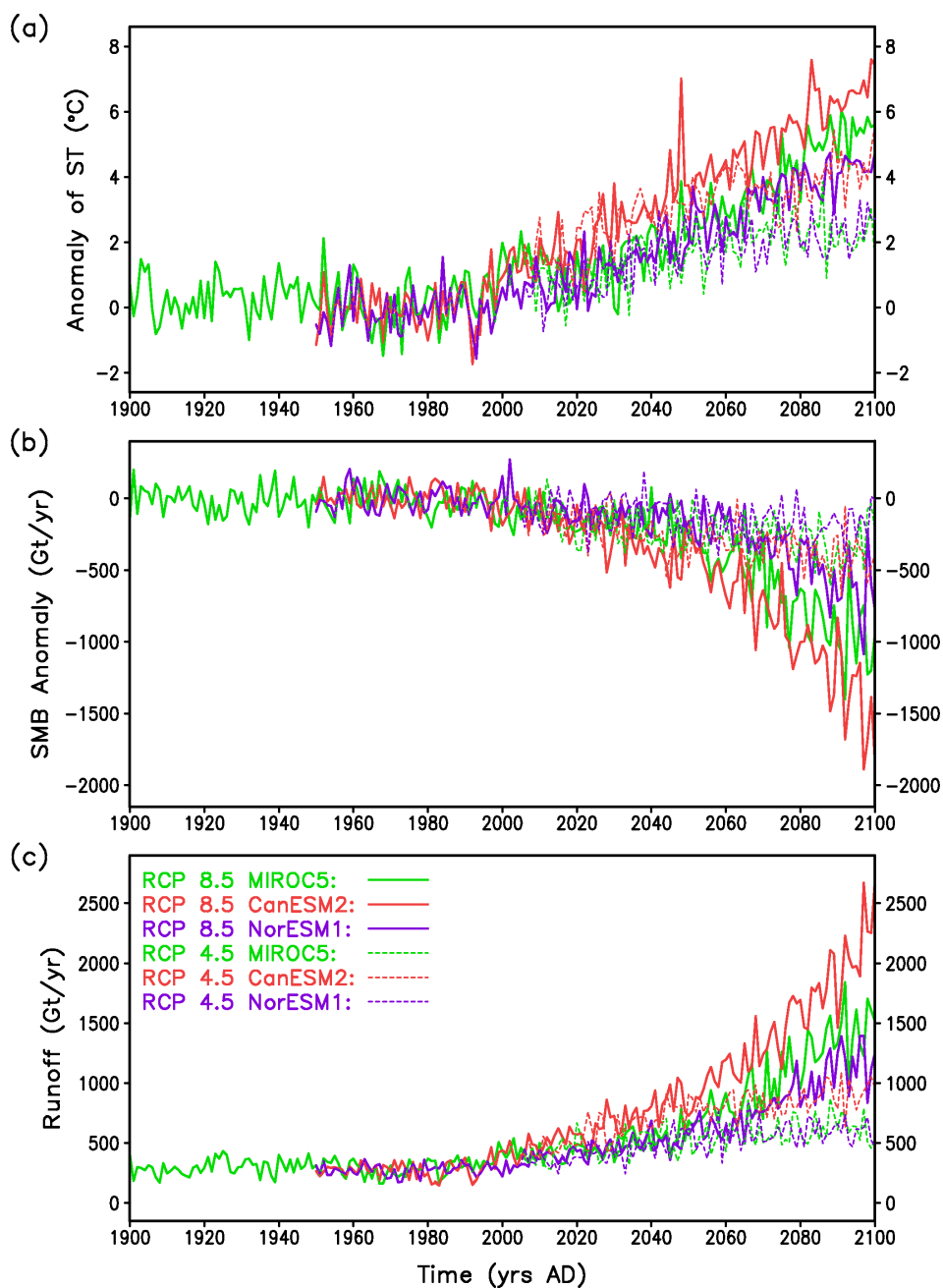


**Figure 2.** Forcings derived from the MAR regional model. (a) Anomaly of annual average surface temperature, (b) total annual surface mass balance anomaly, and (c) total annual runoff. Anomalies are taken with respect to the period 1961–1990 from the respective CMIP5 models. RCP 8.5 scenarios are indicated by the solid lines, while RCP 4.5 scenarios are shown by the dashed lines.

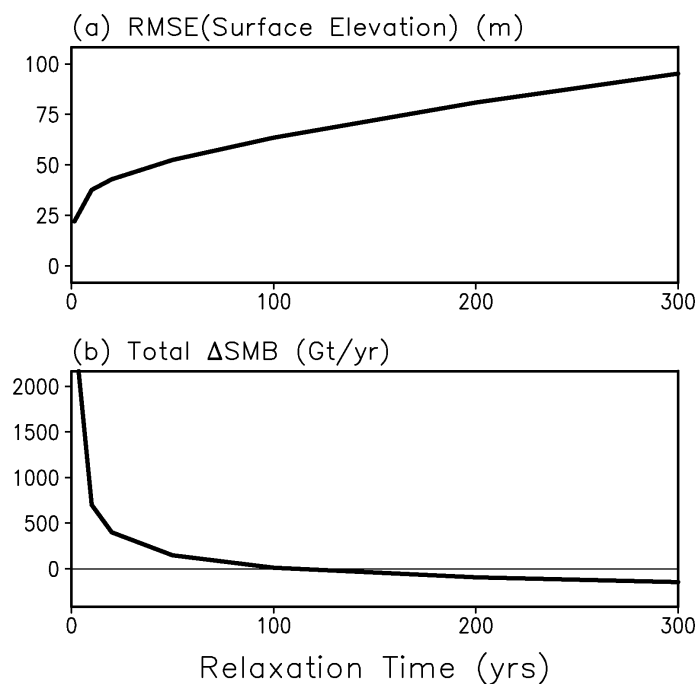


**Figure 3.** Total ice sheet quantities against relaxation constant. (a) Root mean square error (RMSE) of modelled to observed surface elevation. (b) Total difference between our simulated surface mass balance and the surface mass balance from the regional model MAR using ERA reanalysis 1961-1990 climatology.

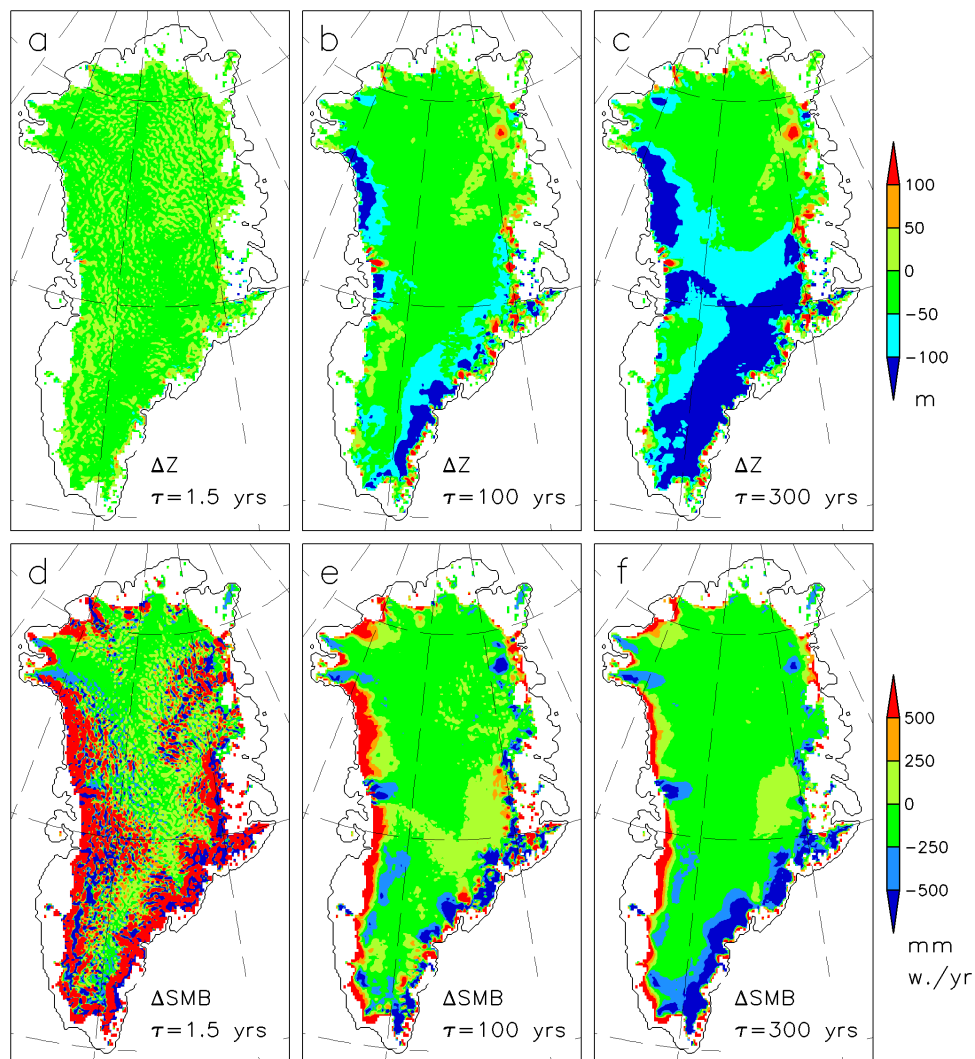


**Figure 4.** Differences between simulated and observed present-day 2-D fields for various relaxation constants, i. e., 1.5, 100 and 300 years. (a), (b) and (c): deviation of surface elevation from observed. (d), (e) and (f): deviation of our implied surface mass balance from the surface mass balance from the regional model MAR.

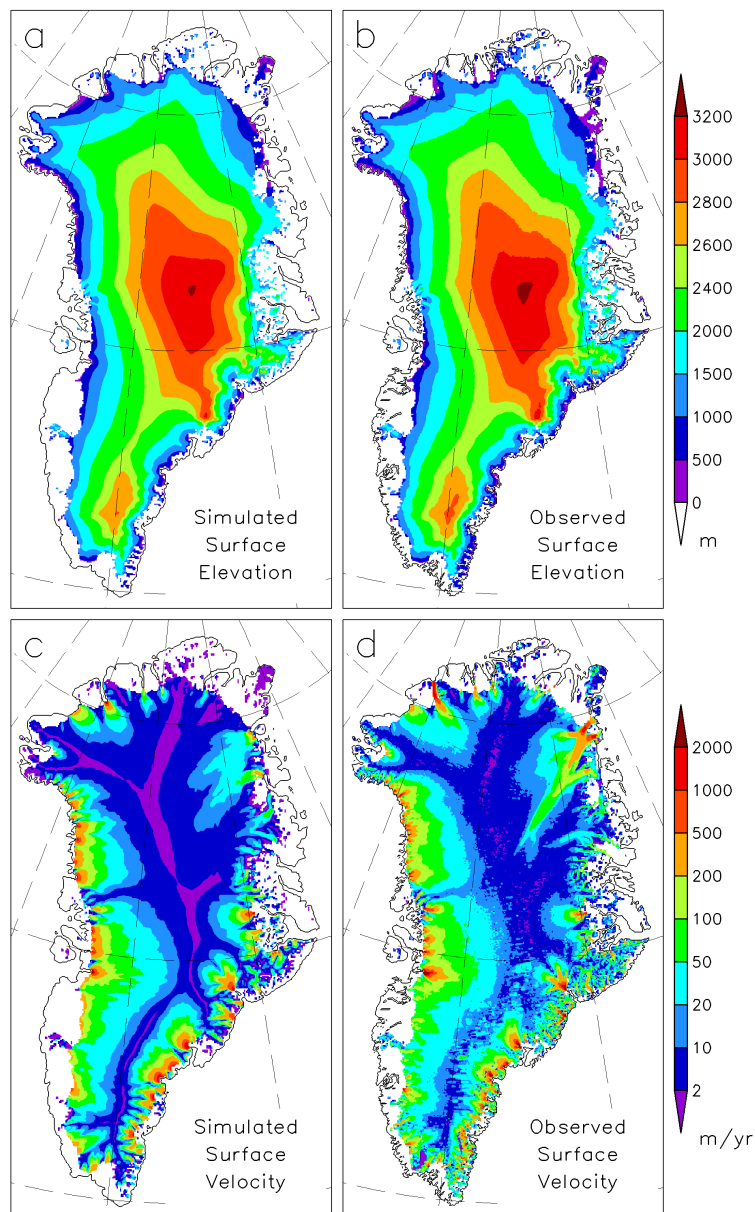


**Figure 5.** Comparison of our simulated with observed 2-D fields for present-day with 100 yrs relaxation constant. (a) Simulated surface elevation, (b) surface elevation by Bamber et al. (2013), (c) simulated horizontal surface velocity, and (d) horizontal surface velocity by Rignot and Mouginot (2012).

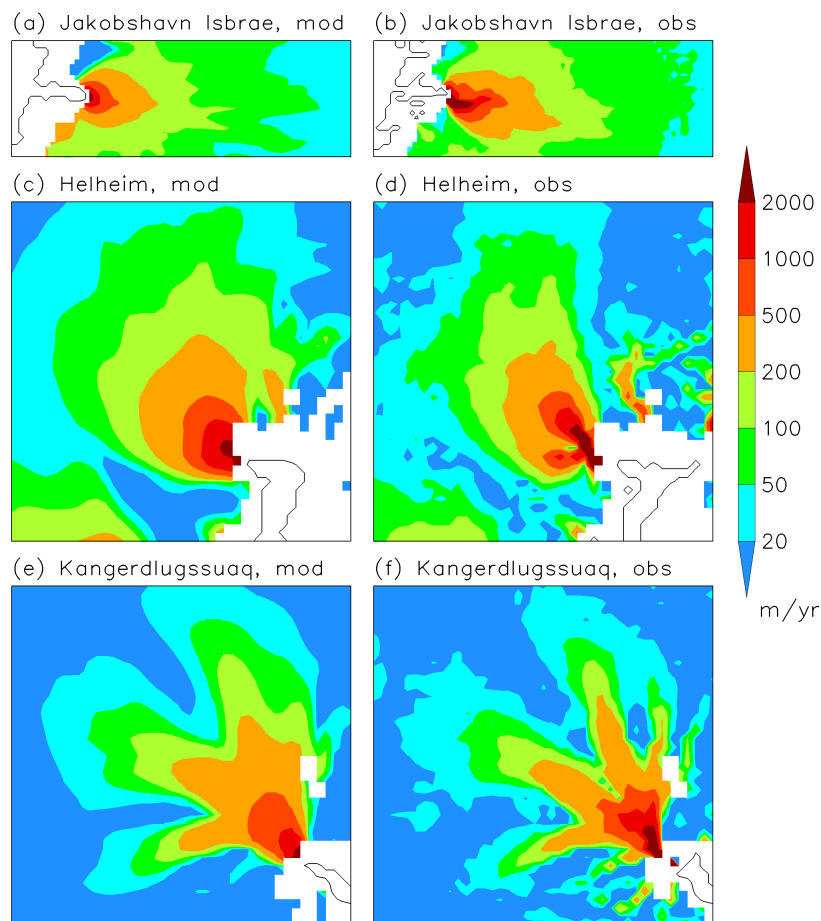


**Figure 6.** Comparison of observed and simulated velocity for major ice streams and outlet glaciers. Left side: modelled, right side: observed. (a, b) Jakobshavn Isbræ, (c, d) Helheim Glacier, and (e, f) Kangerdlugssuaq Glacier.

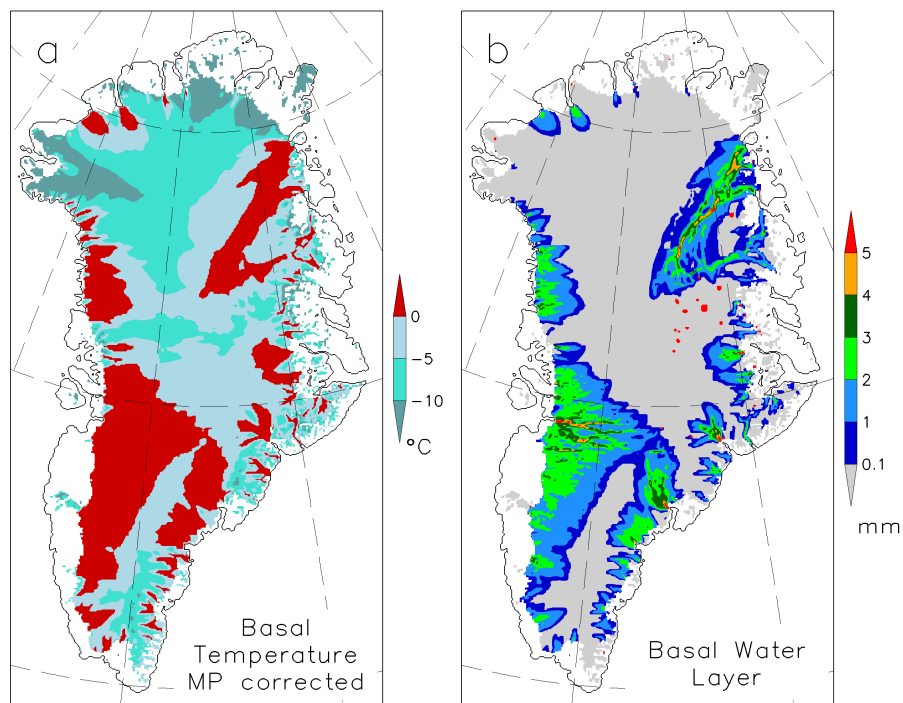


**Figure 7.** Simulated 2-D basal fields. (a) basal temperatures relative to pressure melting (in °C), (b) thickness of basal water layer (in mm).

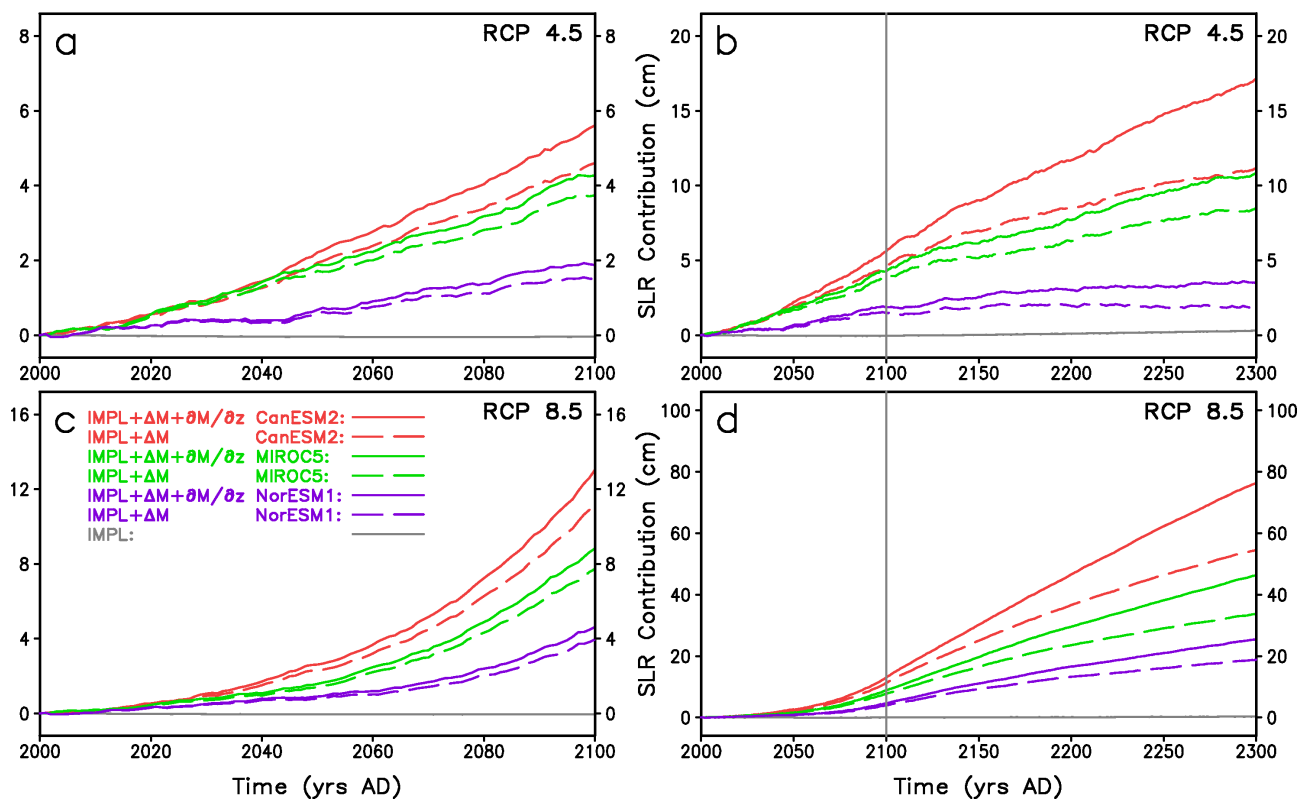


**Figure 8.** Contribution of the Greenland ice sheet to future sea level rise under MAR forcing for different scenarios. Sea level rise is referenced to the year 2000. Beyond 2100, the forcings of the projections are from prolongations of the original MAR data (see main text for details). This is indicated by the vertical grey line at the year 2100 in panels (b) and (d). RCP 4.5 projections: (a) years 2000–2100 and (b) years 2000–2300. RCP 8.5 projections: (c) years 2000–2100 and (d) years 2000–2300. The different CMIP5 general circulation models utilized by MAR are indicated by colours. Different line characteristics specify optimal simulations with (solid) and without (long dashed) elevation correction for the surface mass balance. The grey curves in panels (a) to (d) indicate a control simulation with solely the implied flux as forcing. All simulations are with hybrid ice dynamics and HYDRO basal hydrology.

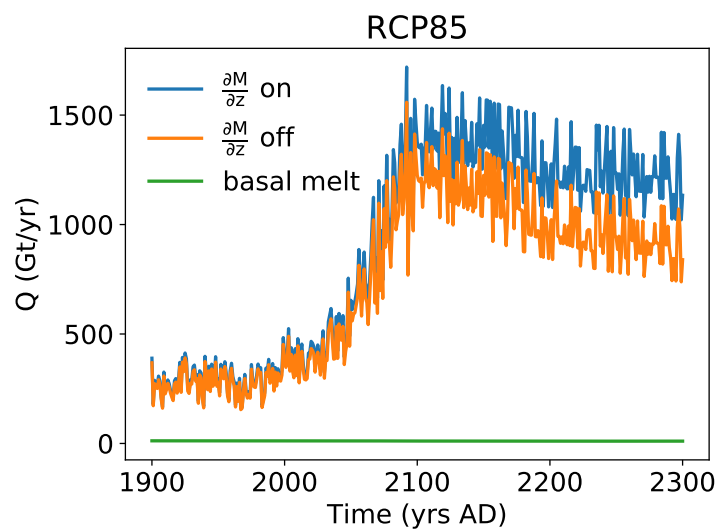


**Figure 9.** Time series of the components of subglacial discharge. The total basal melt (green) amounts to approximately  $15 \text{ Gt yr}^{-1}$ . Total surface runoff with surface elevation SMB feedback (blue) and without the feedback (orange).

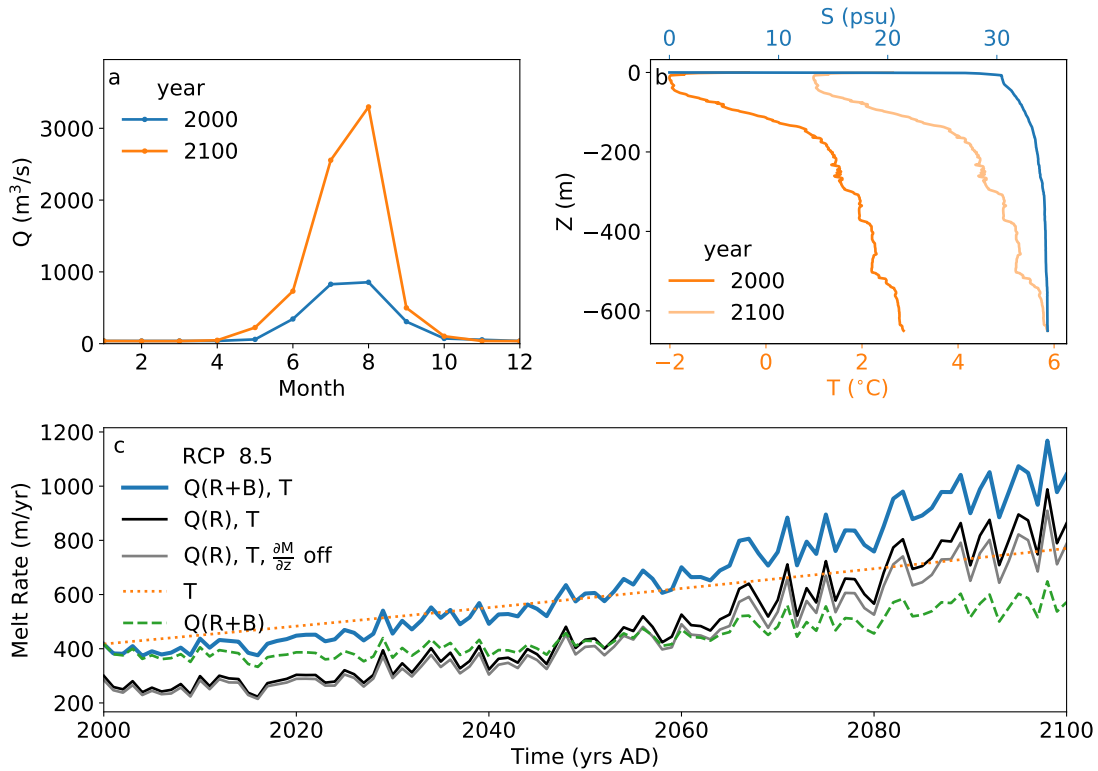


**Figure 10.** a) Monthly subglacial discharge derived from runoff and basal melt (R+B) for Helheim Glacier and the scenario RCP 8.5 in the years 2000 and 2100. b) Temperature-depth and salinity-depth profiles obtained from measurements, with the temperature profile de- and increased by  $0.03^{\circ}\text{C}/\text{a}^{-1}$  for the years 2000 and 2100 (Section 2.8). The corresponding submarine melt rates are depicted in c). The effects of increased temperature and discharge only (orange dotted and green dashed lines respectively), as well as the combined effect (solid lines) are displayed until the year 2100. Melt rates with subglacial discharge or only surface runoff are depicted in black. Melt rates of subglacial discharge containing only surface runoff that was calculated without the surface elevation feedback are depicted in grey.

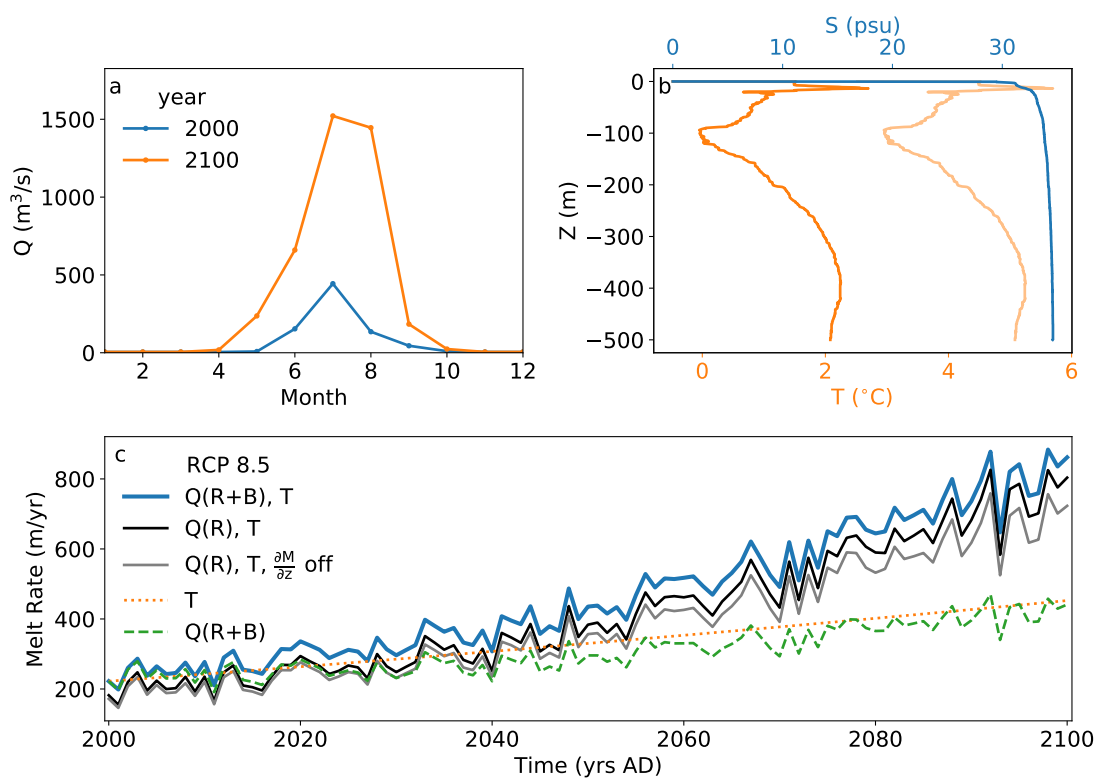


**Figure 11.** Similar to Figure 10, but for Store Glacier.

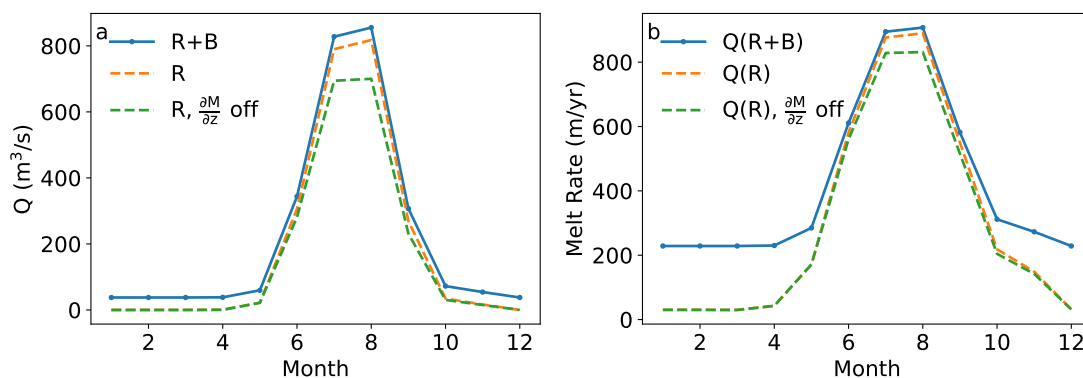


**Figure 12.** Subglacial discharge of Helheim Glacier a) for the year 2000 determined by runoff (R) only (dashed lines), with and without surface elevation feedback (orange, green) and runoff together with basal melt (R+B, blue solid line). The corresponding submarine melt rates b) with the same line colour and line style.